Electronic supplementary information

Pyrene-biimidazole based Ru(II) and Os(II) complexes as highly efficient probes for visible and near-infrared detection of cyanide in aqueous medium

Sourav Mardanya, Srikanta Karmakar, Manoranjan Bar and Sujoy Baitalik*

Department of Chemistry, Inorganic Chemistry Section, Jadavpur University, Kolkata – 700032, India

Physical measurements

Elemental analyses of the compounds were performed with a Vario-Micro V2.0.11 elemental (CHNSO) analyzer. NMR spectra were collected on either a Bruker 300 or Bruker 500 spectrometer in DMSO-d_6, and high resolution mass spectroscopy was performed on a Waters Xevo G2 QTOf mass spectrometer. The UV/vis absorption spectra were recorded with a Shimadzu UV 1800 spectrometer. A matched pair of quartz cuvettes (path length 1 cm) was employed. Steady state luminescence spectra were obtained either by a Perkin–Elmer LS55 or Spex fluorolog-2 spectrofluorometer equipped with DM3000F software. Luminescence quantum yields were determined by using literature method taking $[Ru(bpy)_3]^{2+}$ as the standard. The quantum yields were calculated by using eq S1.

$$\Phi_r = \Phi_{std} \,.\, A_{std}/A_r \,.\, I_r/I_{std} \,.\, \eta_r^2/\eta_{std}^2 \qquad \text{(S1)}$$

where Φr and Φstd are the quantum yields of unknown and standard samples [Φstd=0.089 (at 298 K) and 0.35 (at 77 K) in ethanol-methanol (4:1) at λex=450 nm], Ar and Astd (<0.1) are the solution absorbances at the excitation wavelength (λex), Ir and Istd are the integrated emission intensities, and ηr and ηstd are the refractive indices of the solvent.[S1]

Luminescence lifetime measurements were carried out by using time–correlated single photon counting set up from Horiba Jobin-Yvon. The luminescence decay data were collected on a Hamamatsu MCP photomultiplier (R3809) and were analyzed by using IBH DAS6 software. Cyclic and square-wave voltammetric experiments were performed in deaerated acetonitrile with a BAS epsilon electrochemistry system and a three-electrode set up consisting of a platinum or glassy carbon working electrode, a platinum counter electrode, and Ag/AgCl reference electrode. Tetraethylammonium perchlorate (TEAP) was used as background electrolyte. The potentials reported in this study were referenced against the Ag/AgCl electrode, which under the given experimental conditions gave a value of 0.36 V for the Fc/Fc^+ couple.

Experimental uncertainties were as follows: absorption maxima ± 2 nm; molar absorption coefficients, 10%; emission maxima, ± 5 nm; excited-state lifetimes, 10%; luminescence quantum yields, 20%; redox potentials ± 10 mV.

Anion sensing experiments

For a typical absorption and emission titration experiment, aliquots of a TBA salts of F^-, Cl^-, Br^-, I^- and AcO^- and $H_2PO_4^-$ (5.0×10^{-3} M) were added incrementally to a 2.5 mL solution of the complexes (2.0×10^{-5} M). In aqueous medium the experiments were carried out in

HEPES buffer medium (pH=7.00) and the concentration of the metal complexes were taken as 1.5 × 10^{-5} M for study. The equilibrium constants were evaluated from the absorbance data using equation (S2)[S2].

$$A_{obs} = (A_0 + A_\infty K[G]_T)/(1+ K[G]_T) \quad (S2)$$

where A_{obs} is the observed absorbance, A_0 is the absorbance of the free receptor, A_∞ is the maximum absorbance induced by the presence of a given anionic guest, $[G]_T$ is the total concentration of the guest, and K is the equilibrium constant of the host–guest entity. Binding constants were performed in duplicate, and the average value is reported. The lifetimes of the receptors were recorded as a function of different anions and solvents.

X-ray crystallographic analyses

The crystallographic data, details of data collection, and refinement parameter for the complexes **1** is summarized in Table S1. Single crystals of suitable size were obtained by diffusing toluene to 1:1 acetonitrile-dichloromethane solution of the complexes. The crystal was immersed in paratone oil and then mounted on the tip of a glass fiber and cemented using epoxy resin. Intensity data for the crystal was collected using MoKα (λ = 0.7107 Å) radiation on a Bruker SMART APEX II diffractometer equipped with CCD area detector at room temperature. The data integration and reduction were processed with SAINT[S3] software provided with the software package of SMART APEX II. An empirical absorption correction was applied to the collected reflections with SADABS.[S3] The structure was solved by direct methods using SHELXTL [S4] and was refined on F^2 by the full-matrix least-squares technique using the SHELXL-97 [S5] program package. Graphics were generated using PLATON. [S6] Non-hydrogen atoms were refined anisotropically until the convergence. All the hydrogen atoms were geometrically positioned and treated as riding atoms. In the complex **1** the hydrogen atoms of the lattice water molecules could not be located from the difference Fourier map.

CCDC reference numbers is 1409760 for **1**

Theoretical computational methods

Quantum chemical calculations were performed with the Gaussian 09 program [S7] employing the DFT method with Becke's three-parameter hybrid functional and Lee-Yang-Parr's gradient corrected correlation functional B3LYP level of theory.[S8-S9] The 6-31G(d) basis set was employed for the C, H and N while SDD basis set was used for Ru and Os atoms. [S10] Geometries were fully optimized using the criteria of the respective programs. To compute the UV-vis transition of the compounds, the singlet excited state geometries corresponding to

the vertical excitations were optimized using the time-dependent DFT (TDDFT) scheme starting with the ground state geometries optimized in solution phase.[S11-S14]The excitation energies, computed within the acetonitrile solvent simulated by the CPCM model,[S15] has been determined by using the so-called nonequilibrium approach, which has been designed for the study of the absorption process.[S16-S17] Only singlet-singlet transitions, that is, the spin-allowed transitions, have been taken into account. The geometries of the lowest energy triplet states of the complexes were also optimized in CH_3CN using the CPCM model. Orbital analysis was completed with Gauss View[S18] and Gauss sum 2.2.[S19]

Table S1 Crystallographic data for **1**

Compound	**1**
Formula	C43 H35 N9 Cl2 O10 Ru
fw	1009.77
T (K)	273(2)
Cryst. Syst.	Monoclinic
Space group	P2(1)/c
a (Å)	11.4961(4)
b (Å)	30.8004(10)
c (Å)	12.1865(4)
α (deg)	90.00
β (deg)	90.00
γ (deg)	90.00
V (Å^3)	4315.1(2)
Dc(g cm^{-3})	1.554
Z	4
μ (mm^{-1})	0.557
F(000)	2056.0
θ range (deg)	2.21-27.50
Data/restraints/params	9382/0/588
GOF on F^2	0.703
R_1 [$I > 2\sigma(I)$][a],	0.0590
wR_2 (all data)[b]	0.1800
$\Delta\rho_{max}/\Delta\rho_{min}$ (e Å)	0.568/ -0.693
[a]$R1(F) = [\sum \| \| F_0 \| - \|F_C \| \| / \sum \| F_0 \|]$, [b]wR2 ($F^2$) $= [\sum w(F_0^2 - F_C^2)^2 / \sum w(F_0^2)^2]^{1/2}$	

Table S2 Selected calculated bond distances (Å) and angles (deg) for **1**, **1a**, **1b** in ground state and triplet excited state along with available X-ray crystal data

	1						
	Exptl.	Soln.(1)	Soln.(1a)	Soln.(1b)	Triplet(**1)**	Triplet (1a)	Triplet(1b)
Ru1-N1	2.075(4)	2.102	2.094	2.083	2.099	2.012	2.068
Ru1-N3	2.187(4)	2.264	2.259	2.200	2.268	2.251	2.226
Ru1-N5	2.057(5)	2.100	2.106	2.110	2.100	2.144	2.096
Ru1-N6	2.057(4)	2.103	2.100	2.095	2.104	2.142	2.098
Ru1-N7	2.030(4)	2.086	2.078	2.073	2.087	2.034	2.089
Ru1-N8	2.008(4)	2.067	2.064	2.077	2.066	2.072	2.078
N1-Ru1-N3	76.85(15)	76.95	77.60	77.54	76.84	78.88	77.65
N1-Ru1-N5	173.91(17)	173.52	172.33	171.27	173.63	170.66	173.00
N1-Ru1-N6	97.68(17)	96.00	94.86	94.02	96.14	95.47	96.65
N1-Ru1-N7	88.31(17)	88.74	89.19	89.92	88.64	93.06	89.13
N1-Ru1-N8	89.54(16)	92.25	91.90	91.98	92.27	92.20	91.08
N3-Ru1-N5	107.39(15)	104.60	103.68	104.10	104.74	104.48	106.25
N3-Ru1-N6	88.12(16)	87.25	87.13	87.53	87.12	80.03	88.54
N3-Ru1-N7	96.80(16)	96.42	96.03	95.36	96.52	96.80	95.14
N3-Ru1-N8	166.14(16)	168.30	168.36	167.88	168.26	170.44	167.57
N5-Ru1-N6	78.31(17)	77.87	77.72	77.56	77.86	76.26	77.82
N5-Ru1-N7	95.43(17)	97.28	98.13	98.39	97.24	95.13	96.21
N5-Ru1-N8	86.38(17)	86.62	87.38	87.17	86.55	84.84	85.49
N6-Ru1-N7	173.01(17)	174.57	175.32	175.53	174.55	171.38	173.70
N6-Ru1-N8	96.39(18)	98.53	98.88	99.04	98.55	98.45	98.08
N7-Ru1-N8	79.97(18)	78.59	78.61	78.35	78.60	80.08	79.25

Table S3 Equilibrium constants[a,b] for **1** and **2** towards various anions in acetonitrile and pure aqueous medium at 298 K

In Acetonitrile Medium					
	From Absorption spectra				
	1			**2**	
anion	$K_1(10^6\ M^{-1})$	$K_2(10^6\ M^{-1})$		$K_1(10^6\ M^{-1})$	$K_2(10^6\ M^{-1})$
F^-	4.36	2.63		3.52	2.98
CN^-	3.60	2.33		3.07	2.79
AcO^-	3.01	2.31		2.82	2.30
$H_2PO_4^-$	2.33	----		1.89	---
From Emission spectra					
	1			**2**	
anion	$K_1(10^6\ M^{-1})$	$K_2(10^6\ M^{-1})$		$K_1(10^6\ M^{-1})$	$K_2(10^6\ M^{-1})$
F^-	3.76	3.33		3.39	2.14
CN^-	3.62	2.80		3.06	1.83
AcO^-	3.16	2.68		2.59	1.68
$H_2PO_4^-$	3.02	----		2.89	---
In Aqueous Medium					
	From Absorption spectra				
	1			**2**	
anion	$K_1(10^5\ M^{-1})$	$K_2(10^4\ M^{-1})$		$K_1(10^5\ M^{-1})$	$K_2(10^4\ M^{-1})$
CN^-	3.45	1.34		6.77	1.07
From Emission Spectra					
	1			**2**	
anion	$K_1(10^5\ M^{-1})$	$K_2(10^4\ M^{-1})$		$K_1(10^5\ M^{-1})$	$K_2(10^4\ M^{-1})$
CN^-	2.03	1.03		3.20	1.37

Table S4 Selected calculated bond distances (Å) and angles (deg) for **2**, **2a**, **2b** in ground state and triplet excited state

	2 (sol)			**2** (triplet)		
	Soln.(2)	Soln.(2a)	Soln.(2b)	Triplet(2**)**	Triplet (2a)	Triplet(2b)
Os1-N1	2.107	2.105	2.097	2.078	2.035	2.019
Os1-N3	2.249	2.248	2.198	2.243	2.244	2.197
Os1-N5	2.102	2.104	2.103	2.115	2.137	2.134
Os1-N6	2.106	2.101	2.095	2.137	2.138	2.128
Os1-N7	2.093	2.082	2.076	2.051	2.051	2.062
Os1-N8	2.074	2.069	2.079	2.076	2.088	2.104
N1-Os1-N3	76.18	76.71	76.66	76.87	77.86	77.98
N1-Os1-N5	173.07	171.96	170.89	172.14	170.42	170.45
N1-Os1-N6	96.15	94.99	94.07	97.03	95.59	95.50
N1-Os1-N7	88.54	88.86	89.56	89.39	92.62	92.36
N1-Os1-N8	93.12	92.77	92.70	93.09	92.76	92.84
N3-Os1-N5	105.24	104.26	104.53	106.74	105.74	105.45
N3-Os1-N6	86.70	86.54	86.99	85.05	85.45	85.59
N3-Os1-N7	96.90	96.41	95.45	97.29	97.13	96.83
N3-Os1-N8	168.31	168.26	167.52	169.54	169.87	169.77
N5-Os1-N6	77.25	77.16	77.05	76.56	76.06	76.07
N5-Os1-N7	97.95	98.91	99.24	96.95	95.67	96.00
N5-Os1-N8	85.93	86.88	87.00	83.57	84.11	84.33
N6-Os1-N7	174.66	175.60	176.00	173.51	171.73	172.08
N6-Os1-N8	99.28	99.72	100.43	99.28	99.44	99.93
N7-Os1-N8	77.87	77.93	77.72	79.42	79.27	78.85

Table S5 Selected molecular orbital along with their energies and compositions for **1, 1a, 1b** and **2**, **2a** and **2b** in triplet excited state (using 6-31G(d) and SDD basis sets)

	Energy/ eV			(%) Composition											
				1 (%) Composition				**1a** (%) Composition				**1b** (%) Composition			
MO	**1**	**1a**	**1b**	Ru^{II}	pyrene imida	imida	bpy	Ru^{II}	pyrene imida	imida	bpy	Ru^{II}	pyrene imida	imida	bpy
LUMO+3	-1.95	-1.47	-1.16	3.87	62.23	31.63	2.25	2.64	1.07	0.27	96.00	1.70	79.97	0.05	18.26
LUMO+2	-2.18	-1.64	-1.34	0.48	91.23	7.72	0.55	0.61	97.83	0.46	1.07	2.90	1.48	0.16	95.45
LUMO+1	-2.46	-2.27	-2.15	6.04	0.38	0.05	93.50	4.83	0.44	0.09	94.63	6.75	0.54	0.08	92.61
LUMO	-2.52	-2.62	-2.5	3.10	0.44	0.53	95.91	7.15	0.10	0.45	92.29	5.70	0.07	0.30	93.91
HOMO	-5.43	-5.05	-4.12	4.38	88.79	6.22	0.58	26.62	38.23	29.95	5.17	3.44	59.85	36.14	0.55
HOMO-1	-5.92	-5.42	-5.17	75.38	9.67	4.40	10.53	43.27	32.04	15.96	8.72	62.08	13.58	14.47	9.85
HOMO-2	-6.11	-5.76	-5.3	75.22	9.09	1.65	14.02	74.56	2.73	5.12	17.57	59.06	30.72	2.81	7.39
HOMO-3	-6.17	-5.78	-5.43	76.77	2.70	3.55	16.96	71.04	19.08	0.23	9.63	48.82	26.26	10.49	14.41
				2 (%) Composition				**2a** (%) Composition				**2b** (%) Composition			
MO	**2**	**2a**	**2b**	Os^{II}	pyrene imida	imida	bpy	Os^{II}	pyrene imida	imida	bpy	Os^{II}	pyrene imida	imida	bpy
LUMO+3	-1.79	-1.47	-1.2	2.00	92.85	4.38	0.75	2.66	0.76	0.16	96.40	0.99	95.81	0.05	3.14
LUMO+2	-2.05	-1.66	-1.31	3.53	59.59	34.09	2.77	0.61	97.80	0.52	1.05	2.88	1.03	0.17	95.90
LUMO+1	-2.46	-2.27	-2.1	6.73	0.77	0.29	92.19	7.69	0.58	0.14	91.57	8.63	0.56	0.16	90.63
LUMO	-2.82	-2.6	-2.42	7.04	0.68	1.03	91.23	8.66	0.29	0.88	90.15	9.56	0.25	1.01	89.16
HOMO	-5.47	-4.95	-4.35	55.50	25.47	7.84	11.16	48.94	17.17	21.71	12.17	17.17	49.04	28.89	4.88
HOMO-1	-5.78	-5.33	-4.82	24.44	64.56	5.46	5.52	28.35	45.43	19.24	6.96	49.21	22.30	15.43	13.03
HOMO-2	-5.9	-5.56	-5.09	73.07	10.83	1.23	14.85	74.80	5.31	4.39	15.49	62.22	25.95	2.50	9.31
HOMO-3	-5.98	-5.6	-5.25	68.05	5.81	3.66	22.46	59.51	20.17	1.94	18.36	64.26	6.03	5.81	23.88

Table S6 Phosphorescence emissions of **1**, **1a**, **1b** and **2**, **2a and 2b** in acetonitrile solution according to TD-DFT calculation and associated experimental values (using 6-31G(d) and SDD basis sets)

Compounds	Acetonilrile	
	Expt.	Theo. (Transition)
1	712 nm	743 nm L+2 → H (84%), L+2 → H-1 (3%), L+3 → H (8%)
1a	712 nm	849 nm L → H-1 (30%), L → H (65%)
1b	793 nm	1161 nm L → H (96%), L → H-1(3%)
2	786 nm	790 nm L → H-1 (12%), L → H (80%)
2a	806 nm	988 nm L → H (83%) L → H-1 (9%),
2b	834 nm	1200 nm L → H-1 (29%), L → H (63%)

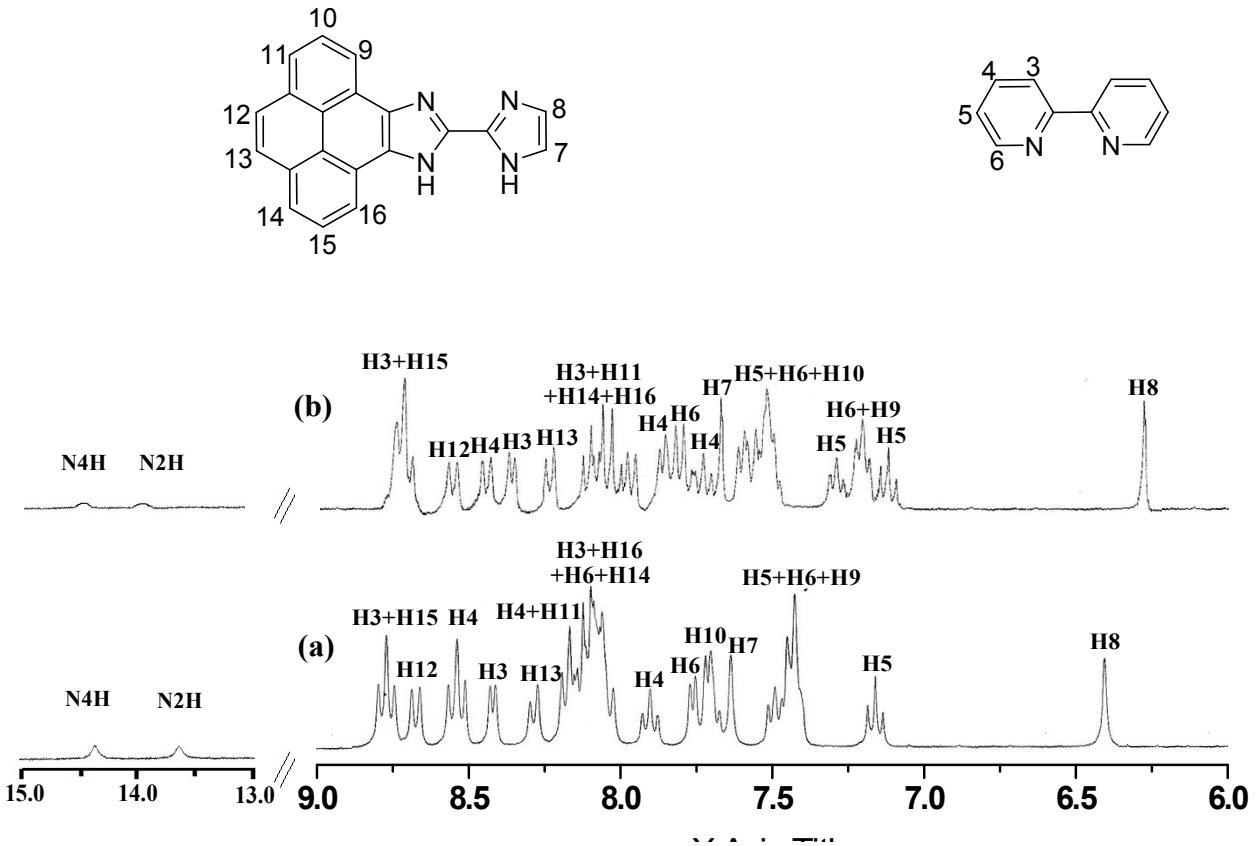

Fig. S1 ^{1}H NMR spectra of **1** (a) and **2** (b) (300 MHz) in DMSO-d_6.

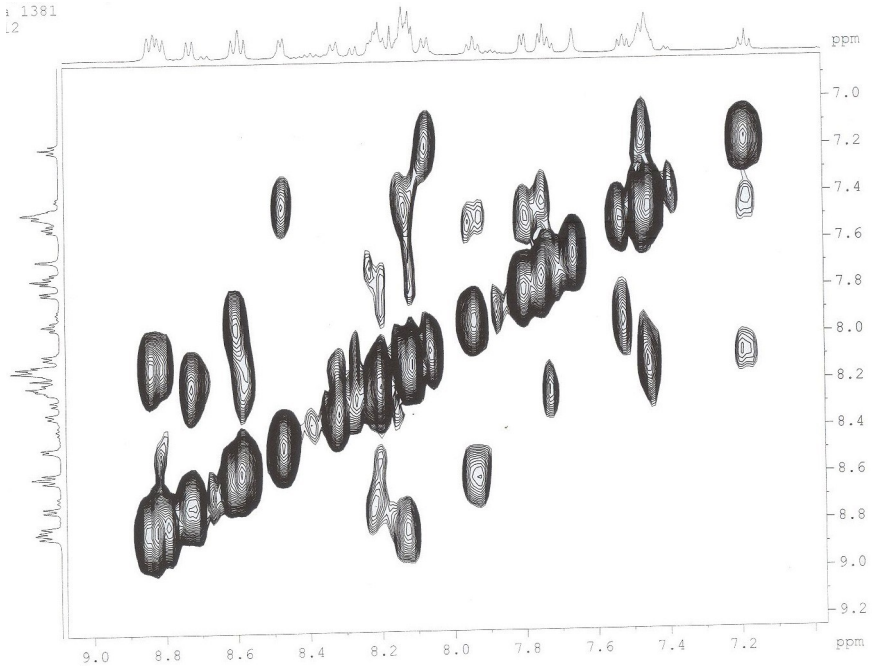

Fig. S2 ^{1}H-^{1}H COSY NMR spectrum of **1** in DMSO-d_6.

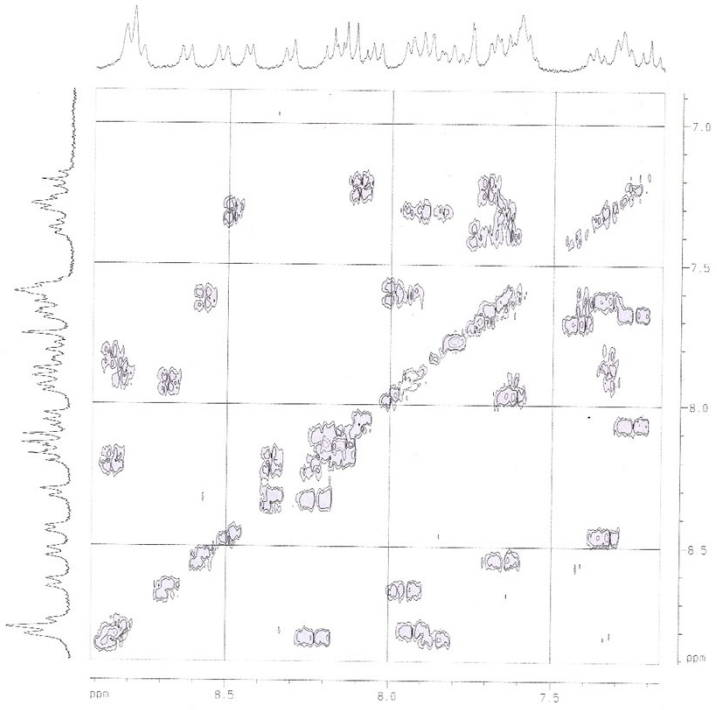

Fig. S3 ^{1}H-^{1}H COSY NMR spectrum of **2** in DMSO-d_6.

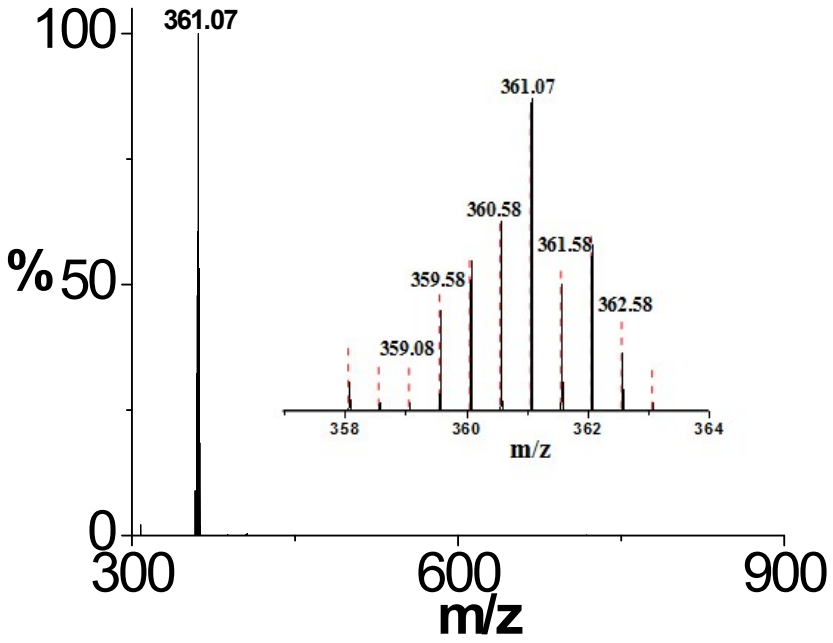

Fig. S4 ESI-MS (positive) for the complex cation $[(bpy)_2Ru(Py\text{-}BiimzH_2)]^{2+}$ (*m/z* = 361.07) in acetonitrile showing the observed and isotopic distribution patterns.

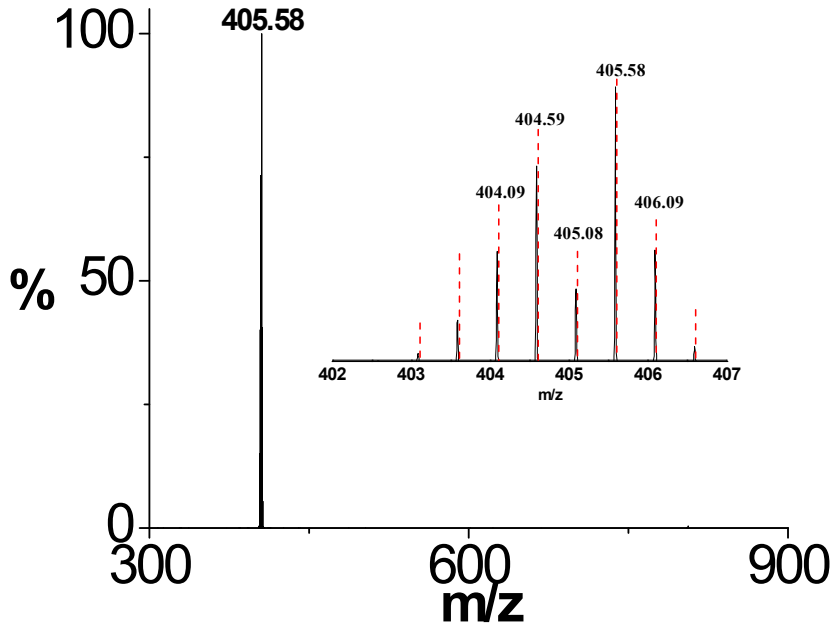

Fig. S5 ESI-MS (positive) for the complex cation $[(bpy)_2Os(Py\text{-}BiimzH_2)]^{2+}$ (*m/z* = 405.58) in acetonitrile showing the observed and isotopic distribution patterns.

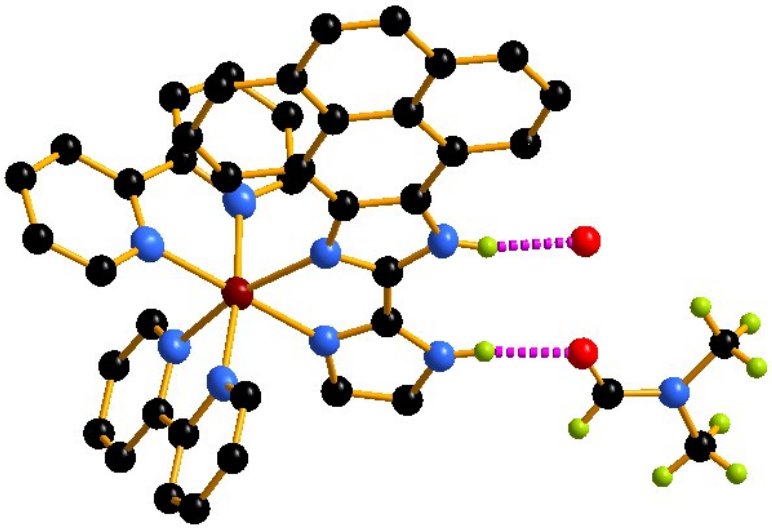

Fig. S6 Strong hydrogen bonding interactions between the N-H imidazole protons of receptor **1** with water and dimethylformamide solvents.

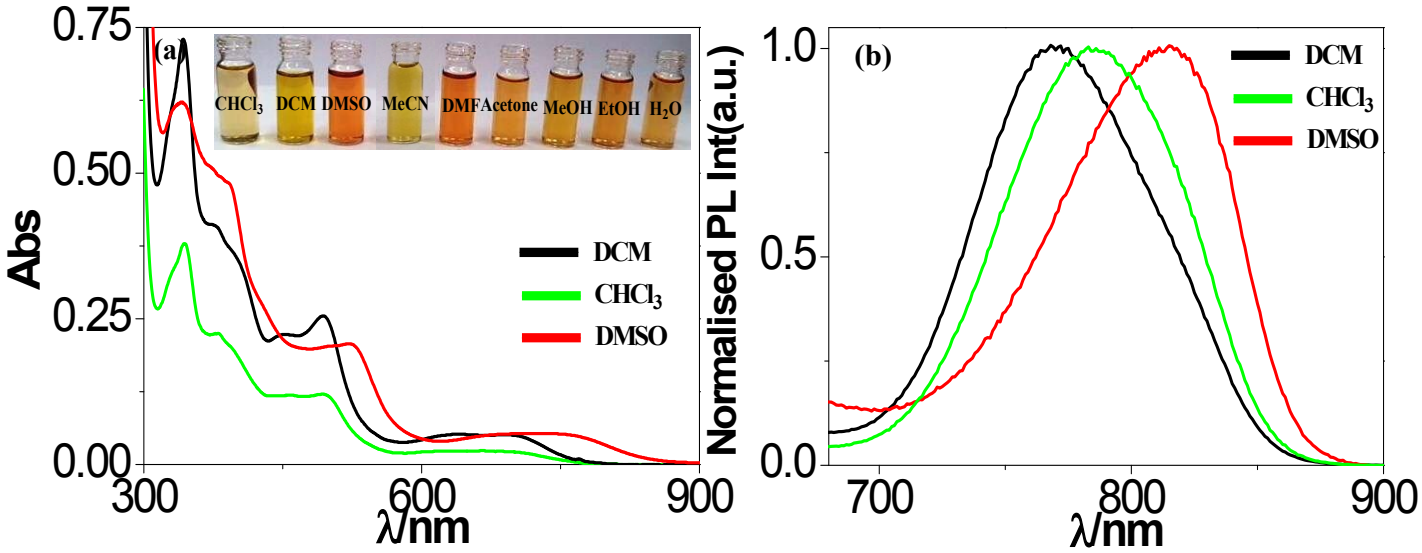

Fig. S7 Changes in UV-vis absorption (a) and emission spectral profiles (b) (normalised) of **2** in few selective solvents.

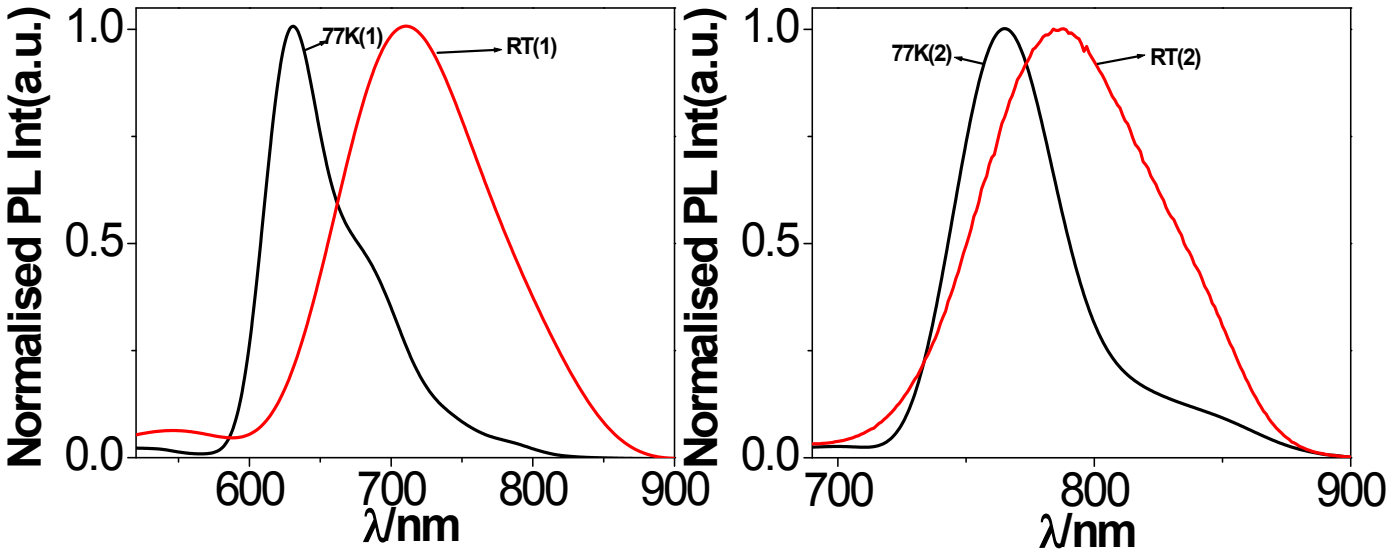

Fig. S8 Luminescence spectra of **1** (a) and **2** (b) in MeCN at room temperature and at 77K in MeOH: EtOH (1:4) glass.

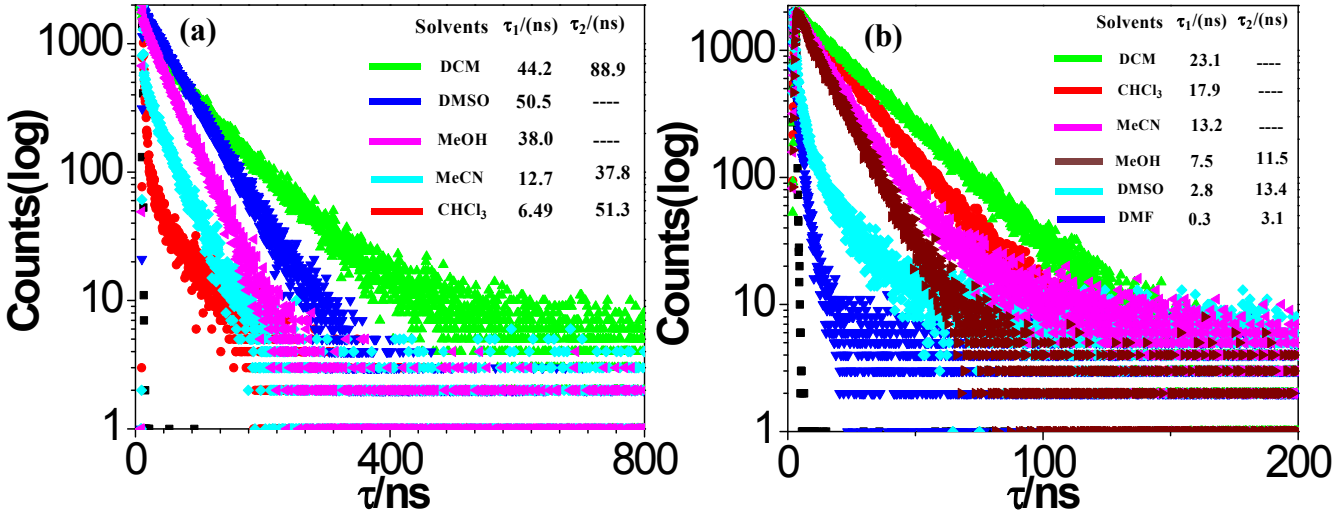

Fig. S9 Decay profiles of **1** (a) and **2** (b) in few selected solvents. Insets show the corresponding lifetimes.

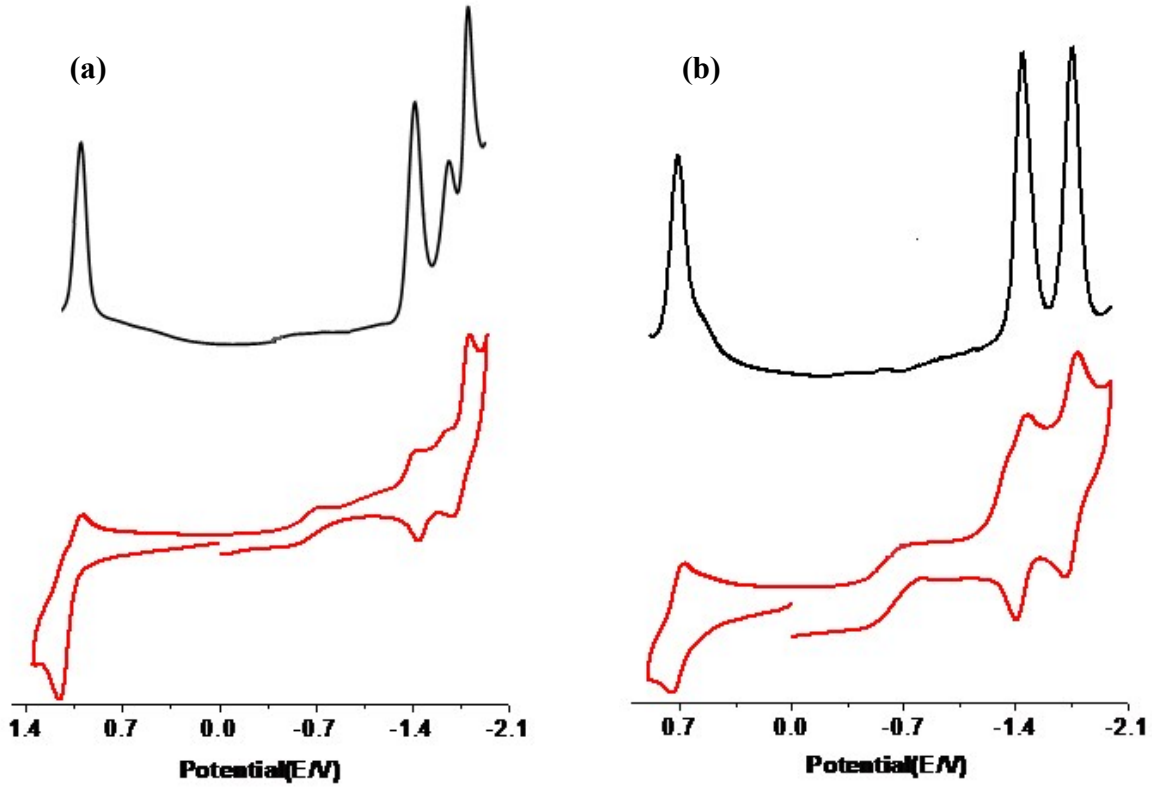

Fig. S10 Cyclic voltammograms and square wave voltammograms of **1** (a) and **2** (b) in acetonitrile at a scan rate of 100 mV/s showing both oxidation and reduction of the complexes.

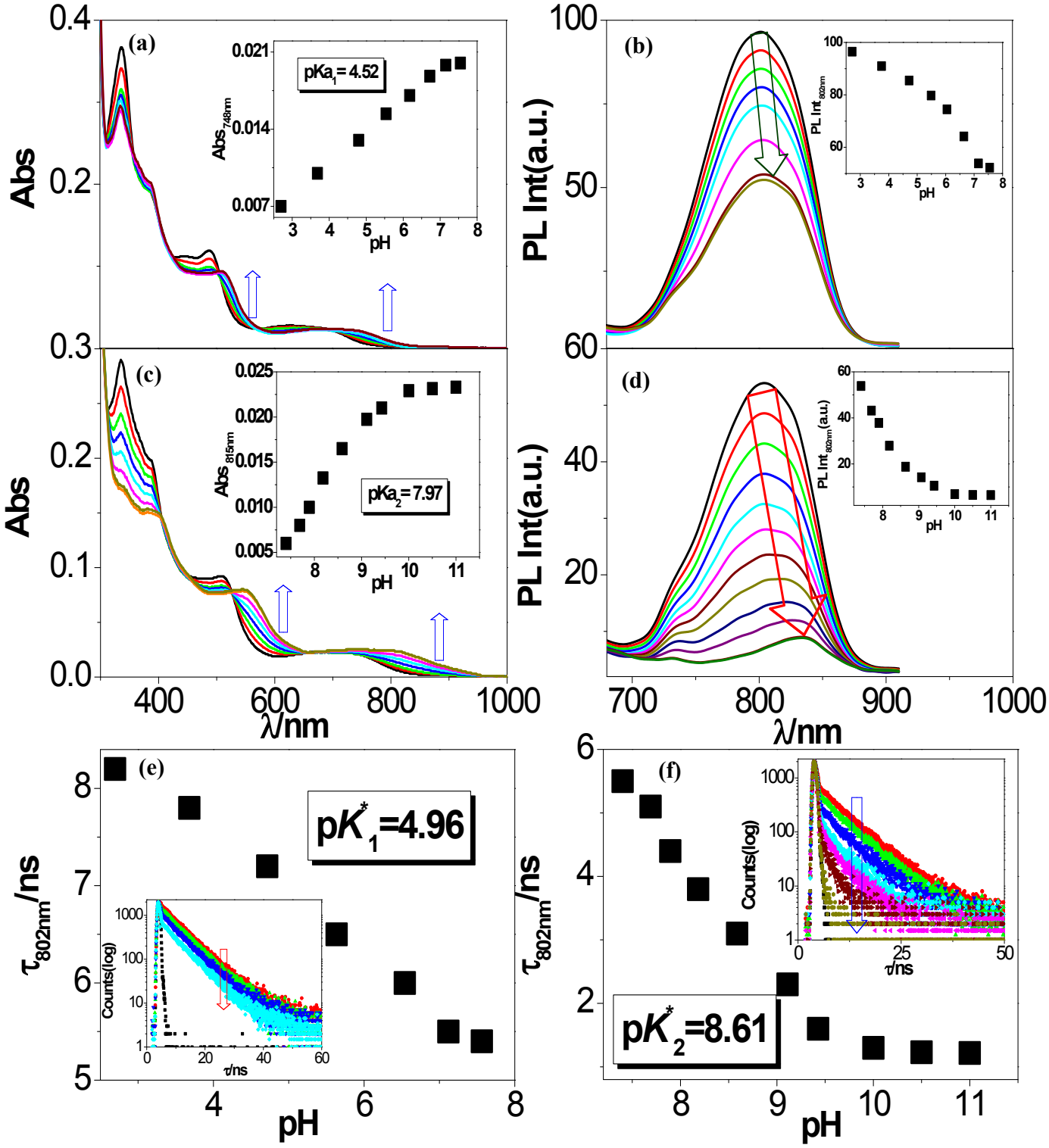

Fig. S11 Changes in absorption, emission and excited state lifetimes of **2** within the pH range 2.5-7.6 (a, b and e) and 7.6-12 (c, d and f) respectively in MeCN/ H_2O (1/9 v/v) mixture. Insets show the variation of absorption, emission and decay profiles with pH.

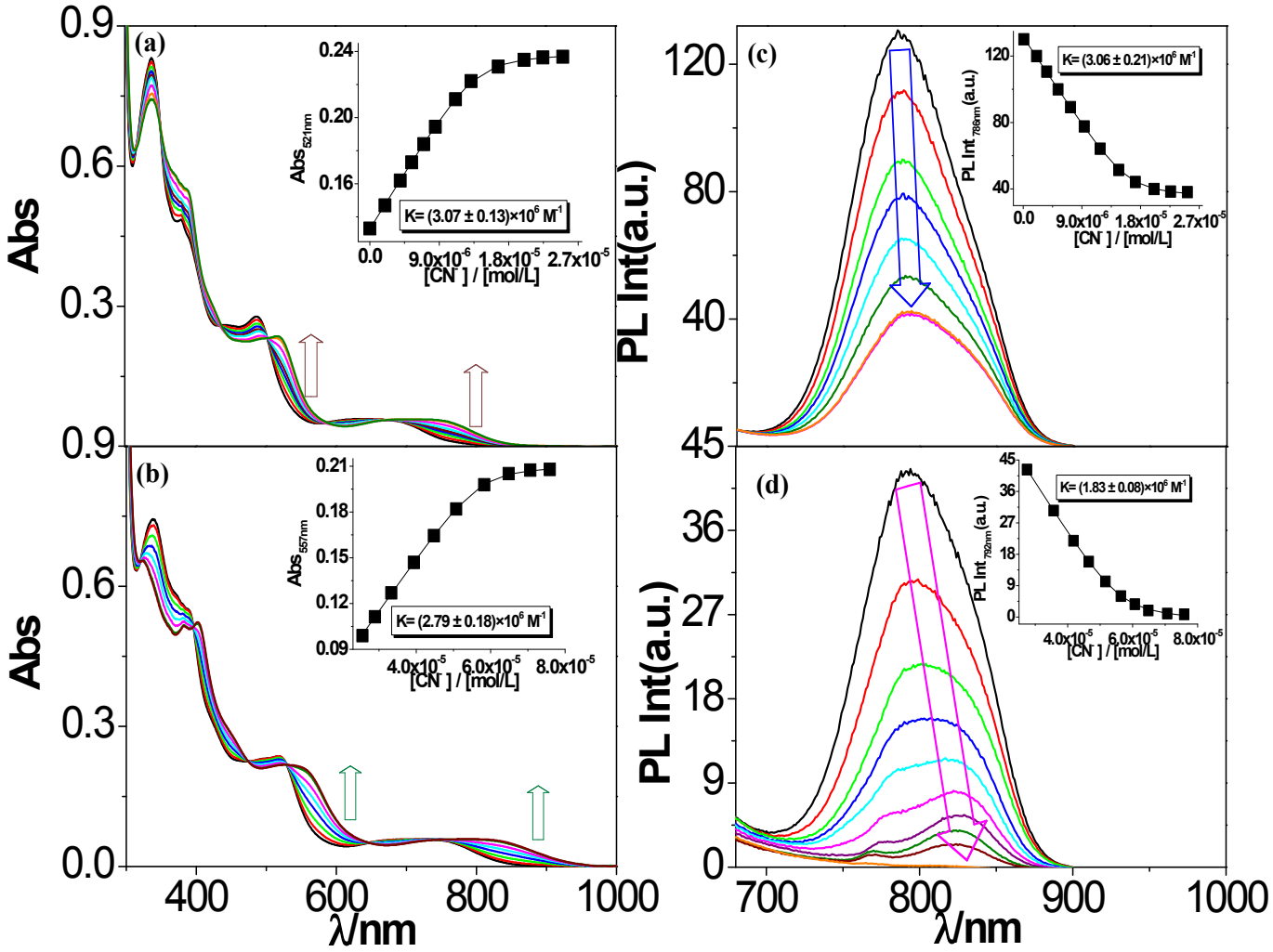

Fig. S12 Changes in UV-vis absorption (a and b) and luminescence (c and d) spectral profiles of **2** in acetonitrile solution upon the addition of CN^- ion. The inset shows the fit of the experimental absorbance and luminescence data to a 1:1 binding profile.

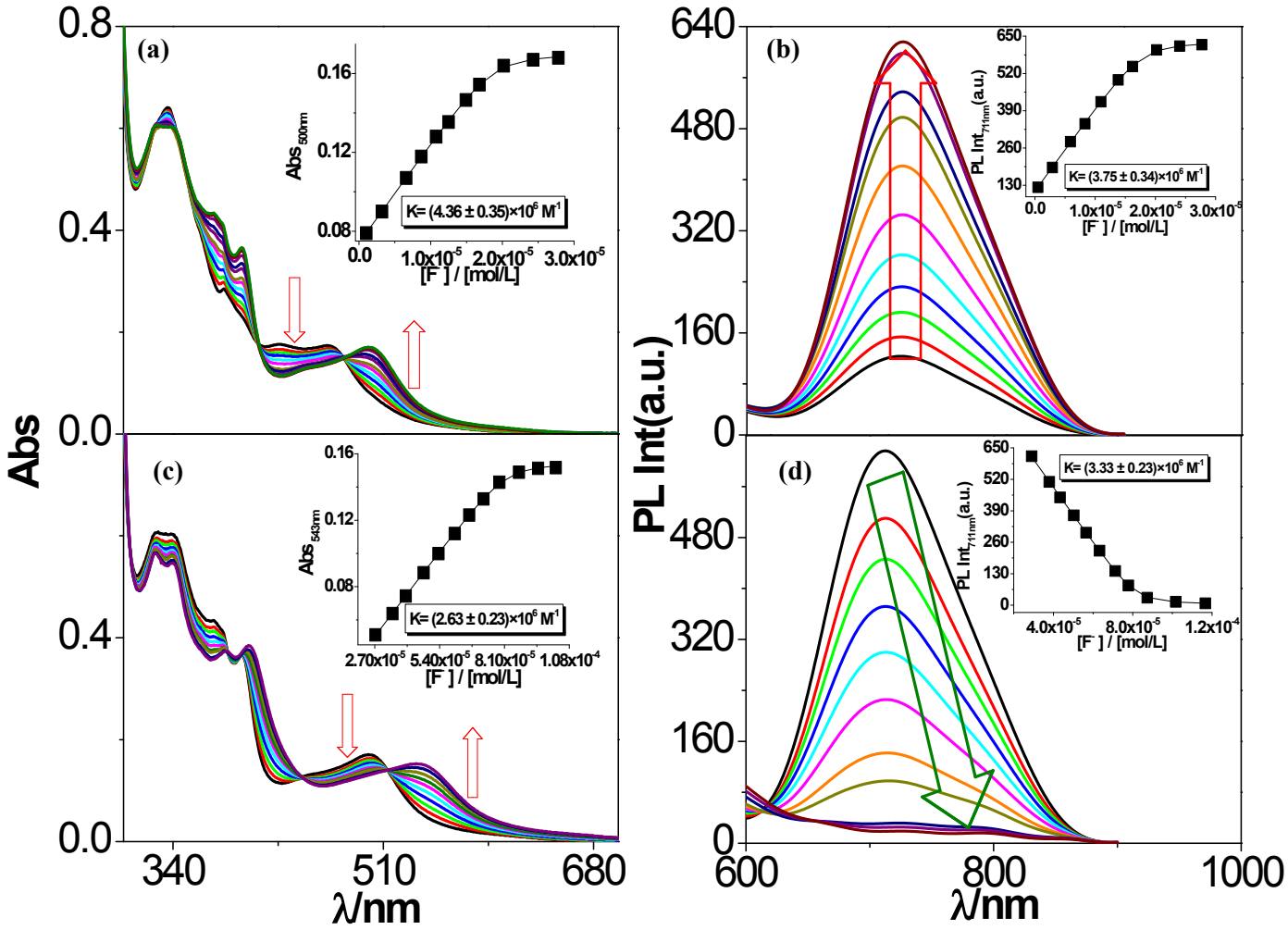

Fig. S13 Changes in UV-vis absorption (a and c) and luminescence (b and d) spectra of complex **1** in acetonitrile solution upon the addition of F^- ion. The inset shows the fit of the experimental absorbance and luminescence data to a 1:1 binding profile.

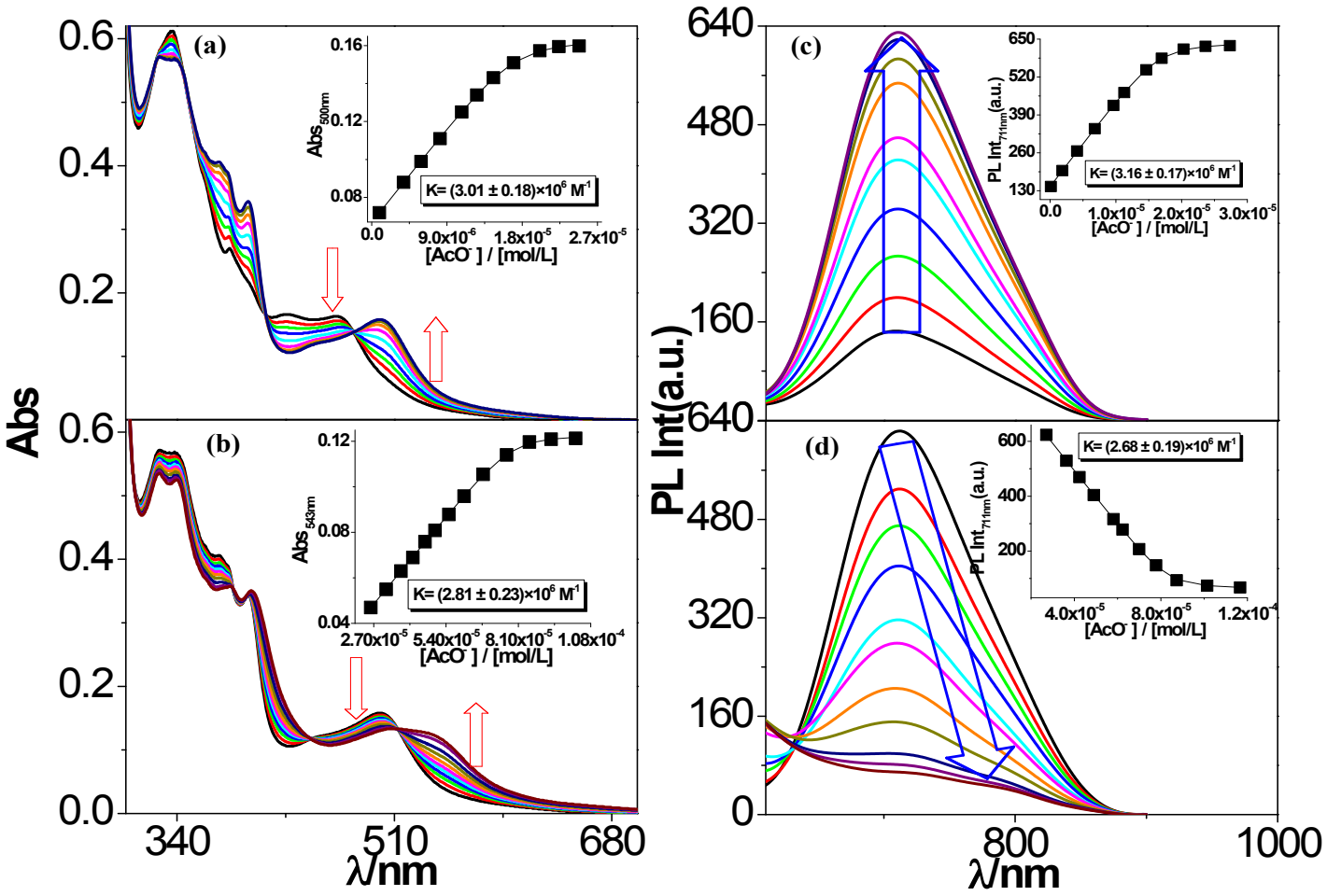

Fig. S14 Changes in UV-vis absorption (a and b) and luminescence (c and d) spectra of complex **1** in acetonitrile solution upon the addition of AcO^- ion. The inset shows the fit of the experimental absorbance and luminescence data to a 1:1 binding profile.

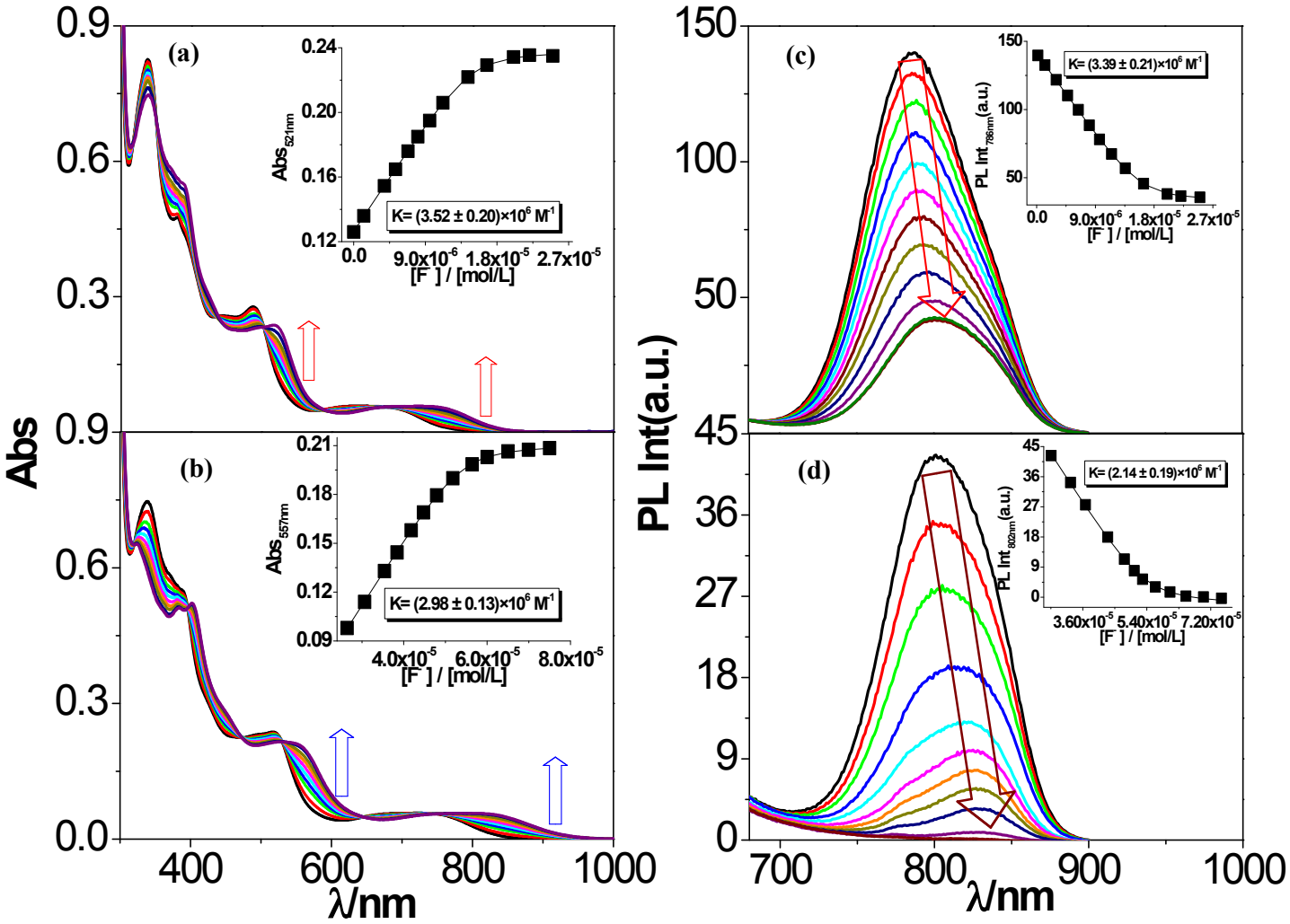

Fig. S15 Changes in UV-vis absorption (a and b) and luminescence (c and d) spectra of complex **2** in acetonitrile solution upon the addition of F^- ion. The inset shows the fit of the experimental absorbance and luminescence data to a 1:1 binding profile.

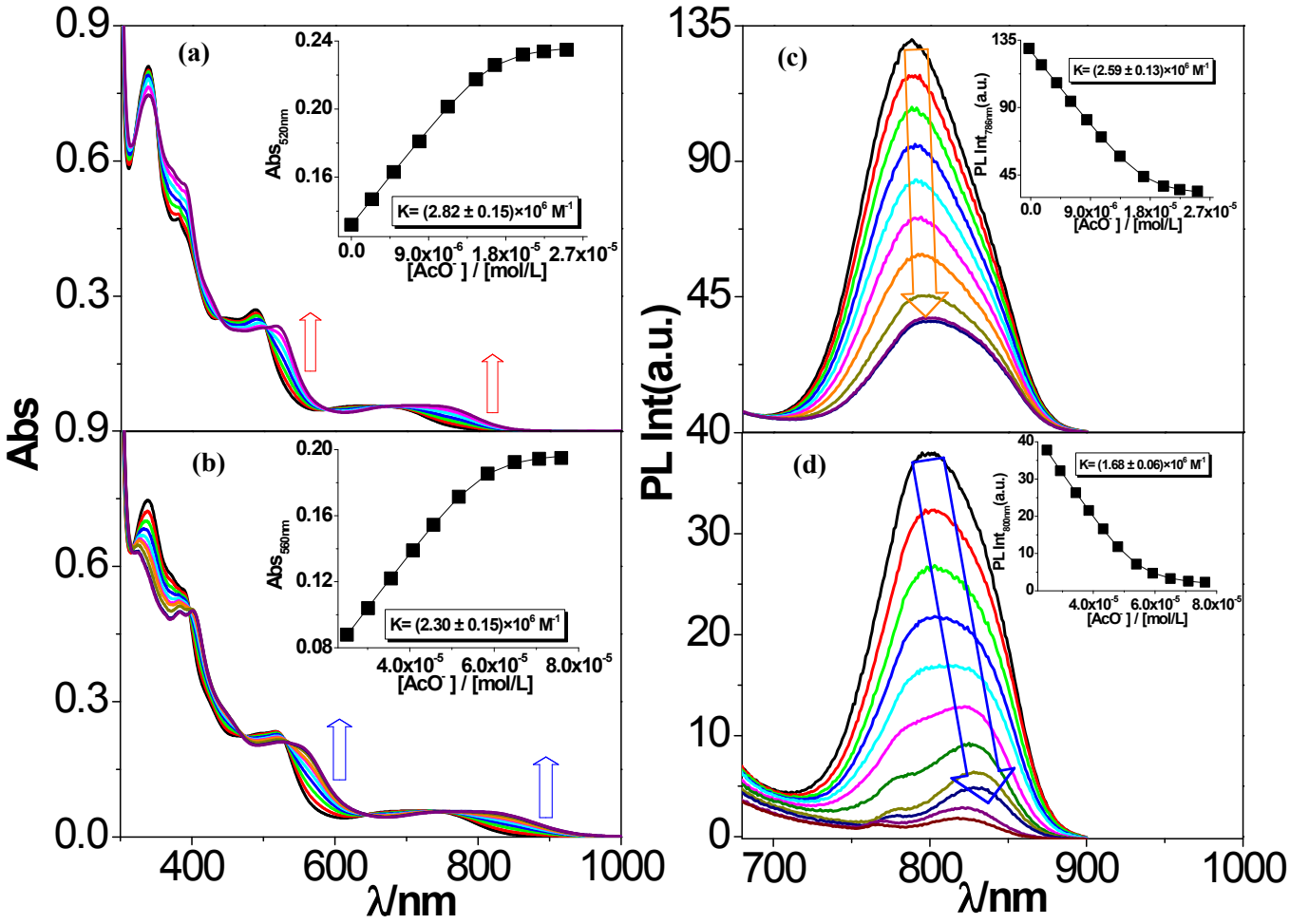

Fig. S16 Changes in UV-vis absorption (a and b) and luminescence (c and d) spectra of complex **2** in acetonitrile solution upon the addition of AcO^- ion. The inset shows the fit of the experimental absorbance and luminescence data to a 1:1 binding profile.

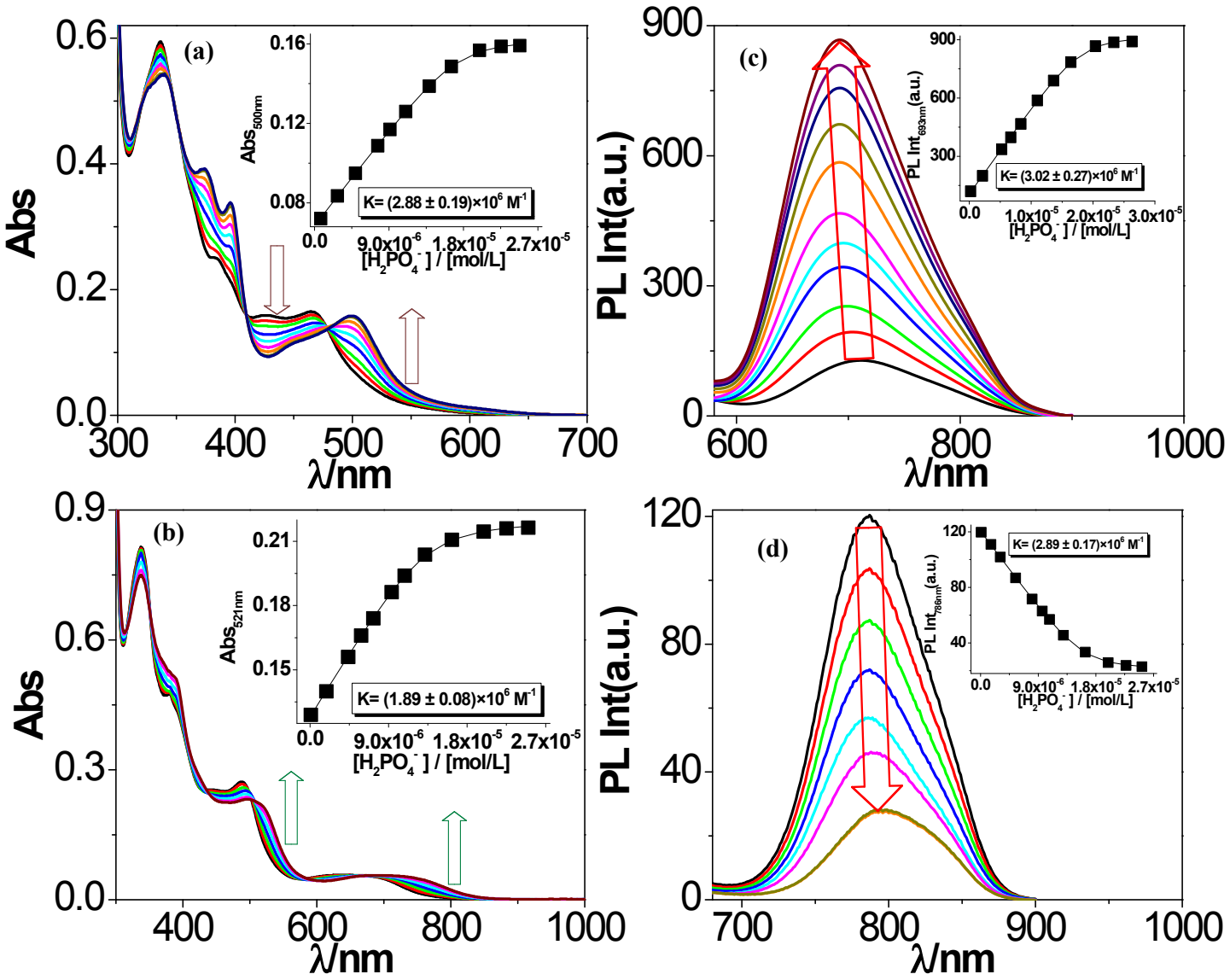

Fig. S17 Changes in UV–vis absorption (a and b) and luminescence (c and d) spectral profiles for **1** and **2**, respectively in acetonitrile solution upon the addition of $H_2PO_4^-$ ion. The inset shows the fit of the experimental absorbance and luminescence data to a 1:1 binding profile.

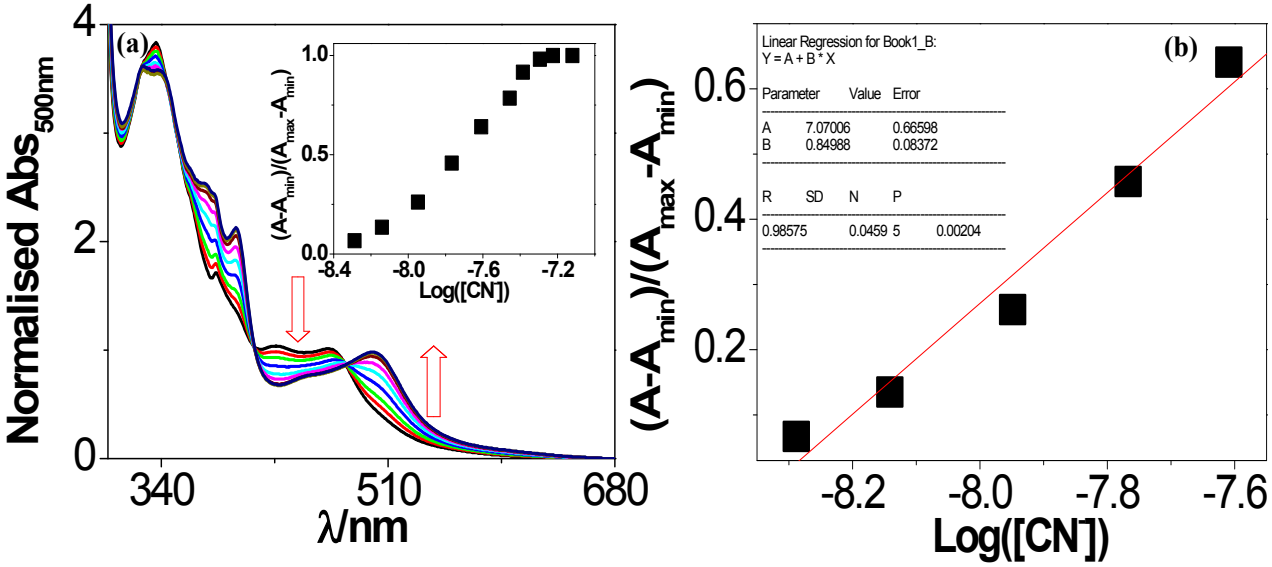

Fig. S18 (a) Absorption spectral change during the titration of **1** with CN^- in acetonitrile, inset shows the normalized absorbance between the minimum absorbance (free complex **1**) and the maximum absorbance. (b) A plot of $(A-A_{min})/(A_{max}-A_{min})$ vs Log([CN^-]), the calculated detection limit of receptor is 5.24×10^{-9} M.

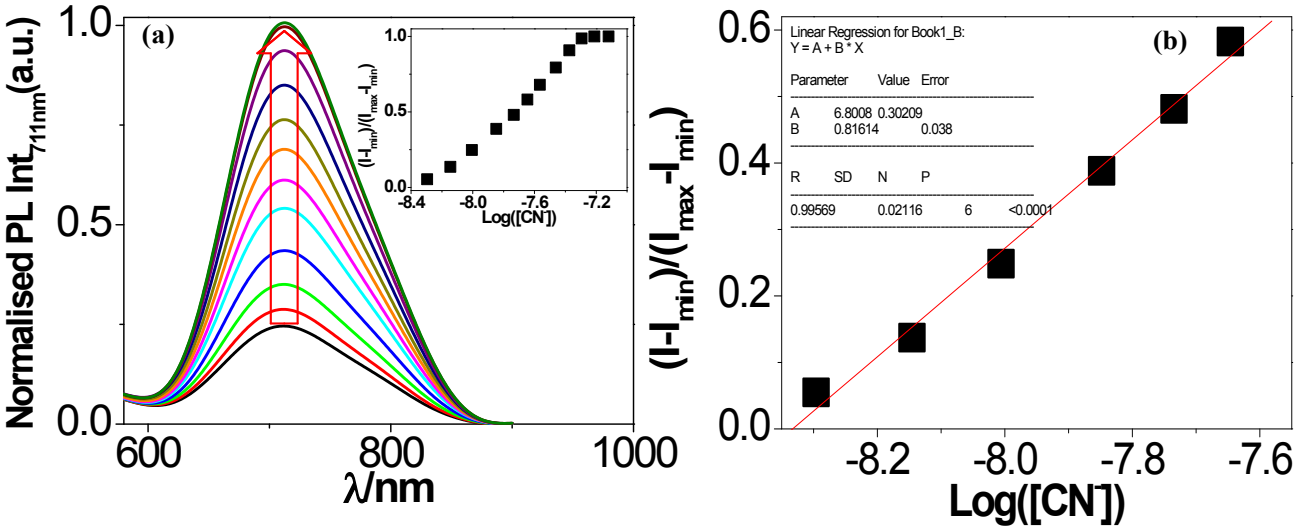

Fig. S19 (a) Fluorescence spectral change during the titration of **1** with CN^- in acetonitrile, inset shows the normalized intensity between the minimum intensity (free complex **1**) and the maximum intensity. (b) A plot of $(I-I_{min})/(I_{max}-I_{min})$ vs Log([CN^-]), the calculated detection limit of receptor is 4.67×10^{-9} M.

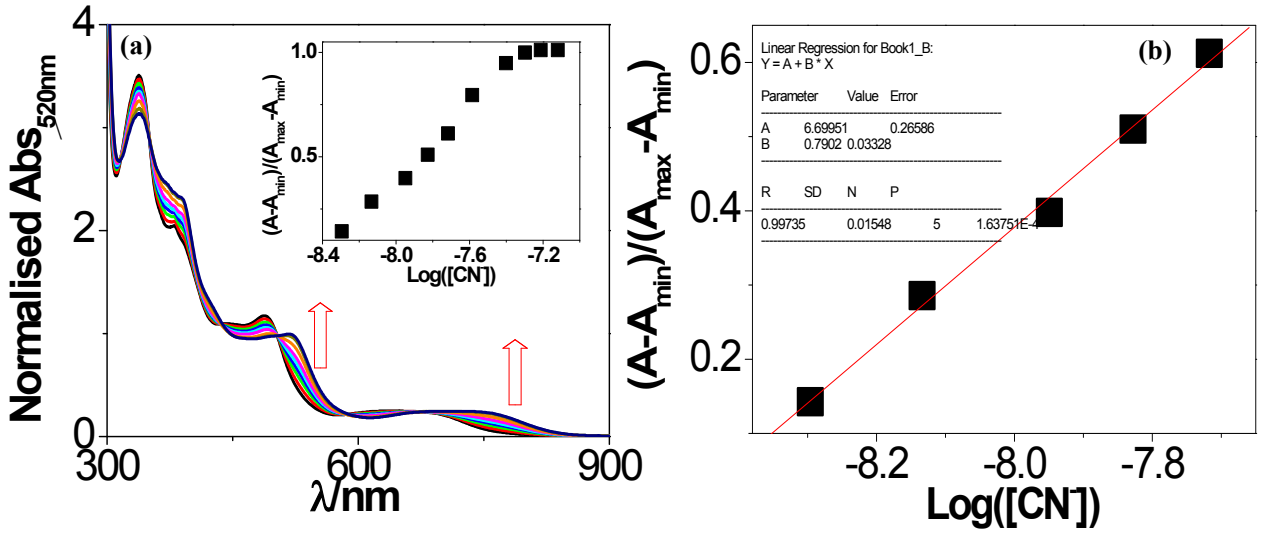

Fig. S20 (a) Absorption spectral change during the titration of **2** with CN^- in acetonitrile, inset shows the normalized absorbance between the minimum absorbance (free complex **2**) and the maximum absorbance. (b) A plot of $(A-A_{min})/(A_{max}-A_{min})$ vs Log([CN^-]), the calculated detection limit of receptor is 4.46×10^{-9} M.

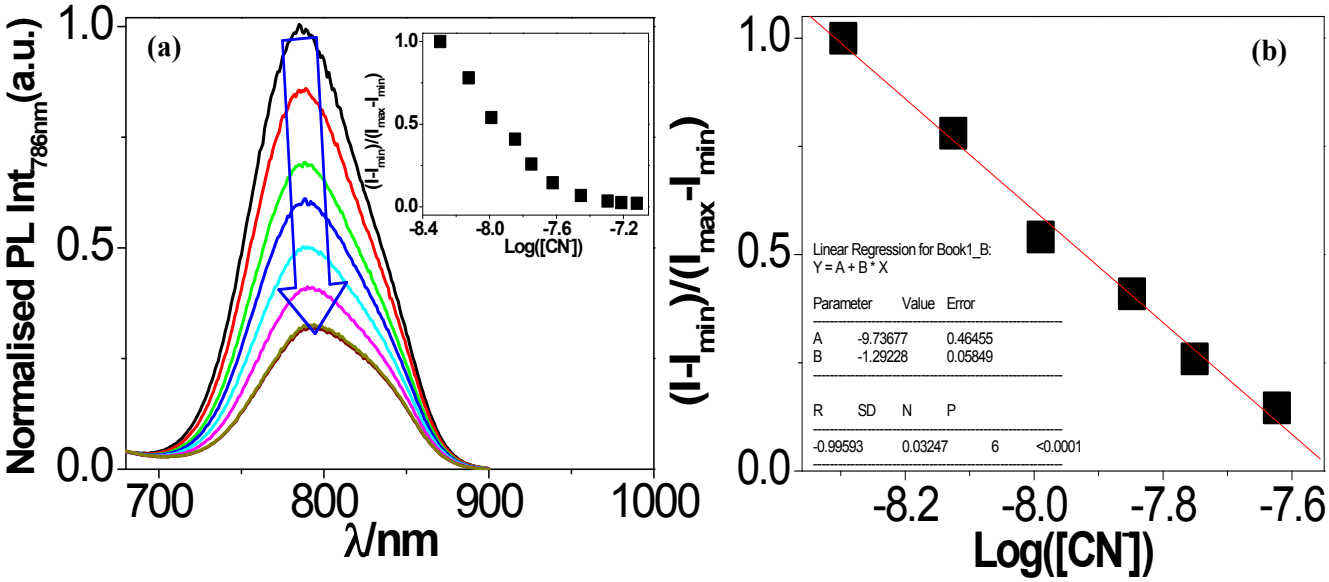

Fig. S21 (a) Fluorescence spectral change during the titration of **2** with CN^- in acetonitrile, inset shows the normalized intensity between the minimum intensity (free complex **2**) and the maximum intensity. (b) A plot of $(I-I_{min})/(I_{max}-I_{min})$ vs Log([CN^-]), the calculated detection limit of receptor is 4.57×10^{-9} M.

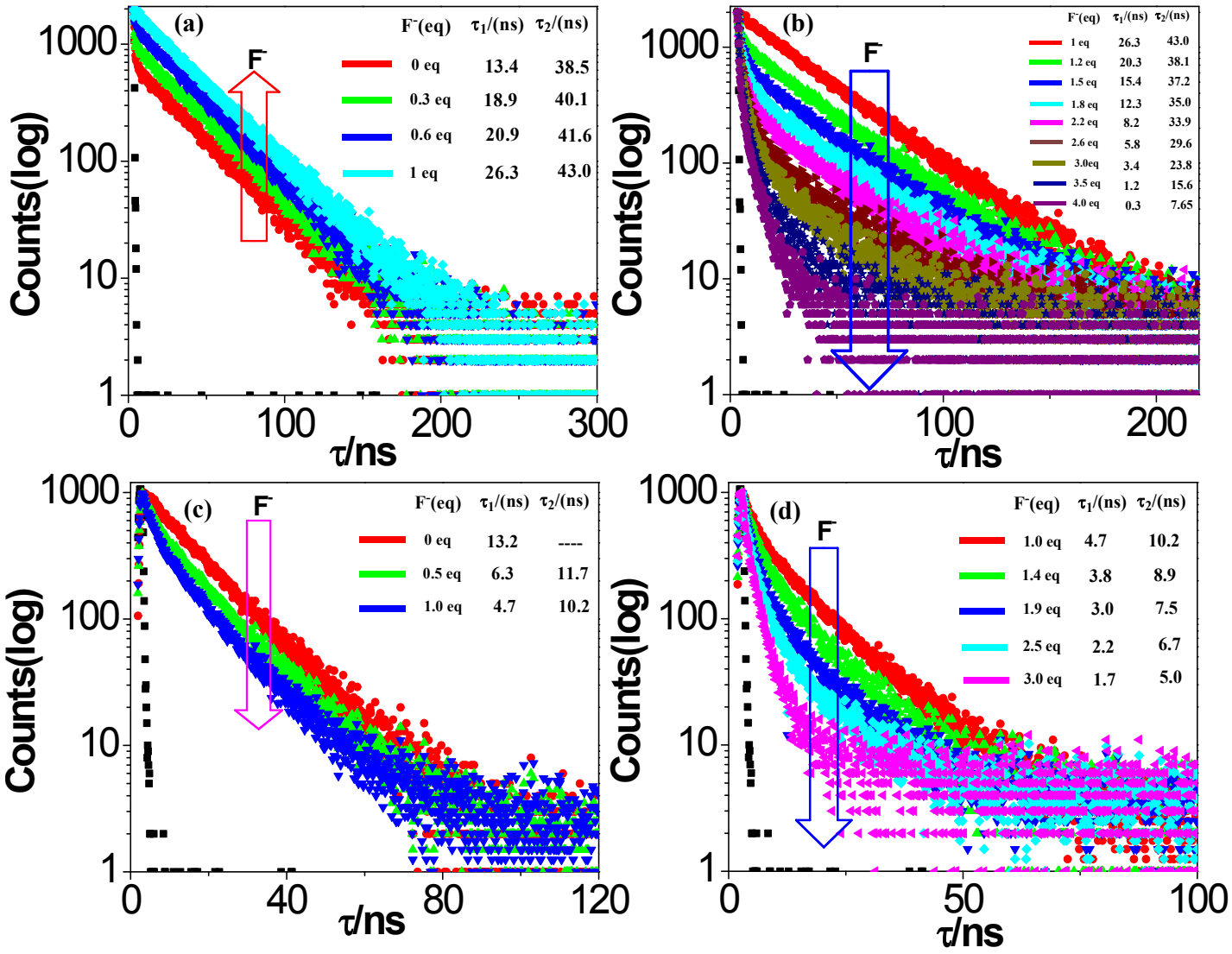

Fig. S22 Changes in the time-resolved luminescence decays for **1** (a and b) with incremental addition of F^- (0-4 equiv) and for **2** (c and d) with F^- (0-3 equiv) in acetonitrile solution. Insets show the lifetime values.

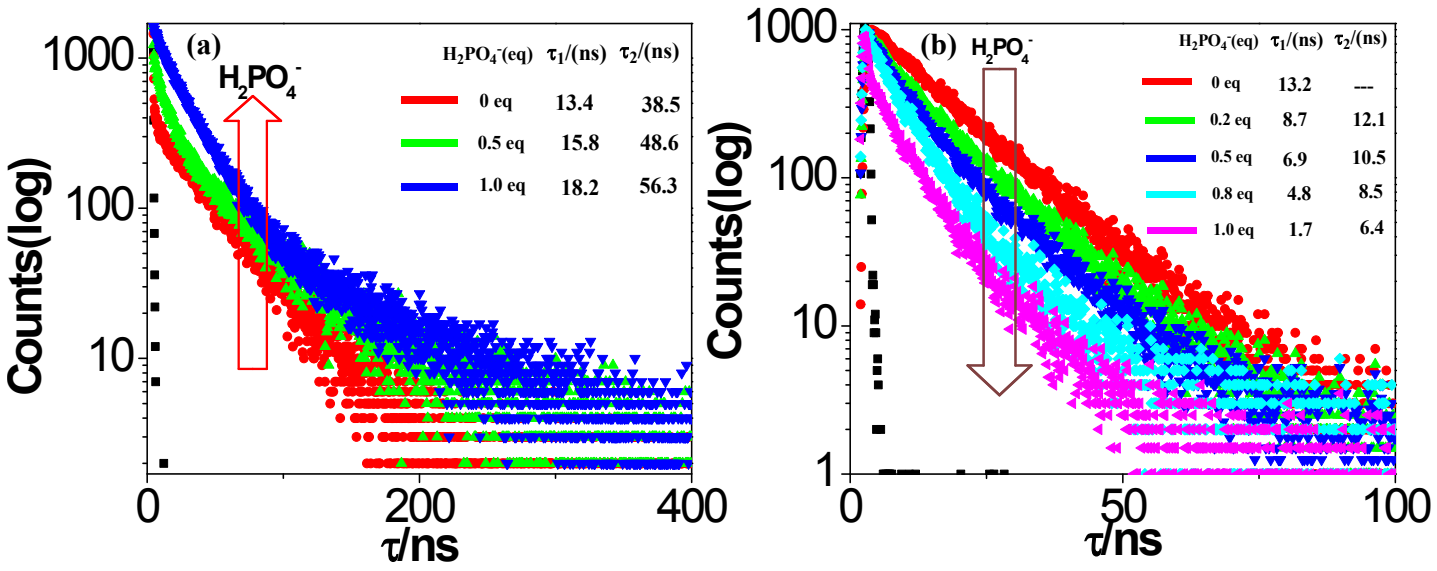

Fig. S23 Changes in the time-resolved luminescence decays for **1** (a) and **2** (b) with incremental addition of $H_2PO_4^-$ in acetonitrile solution. Insets show the lifetime values.

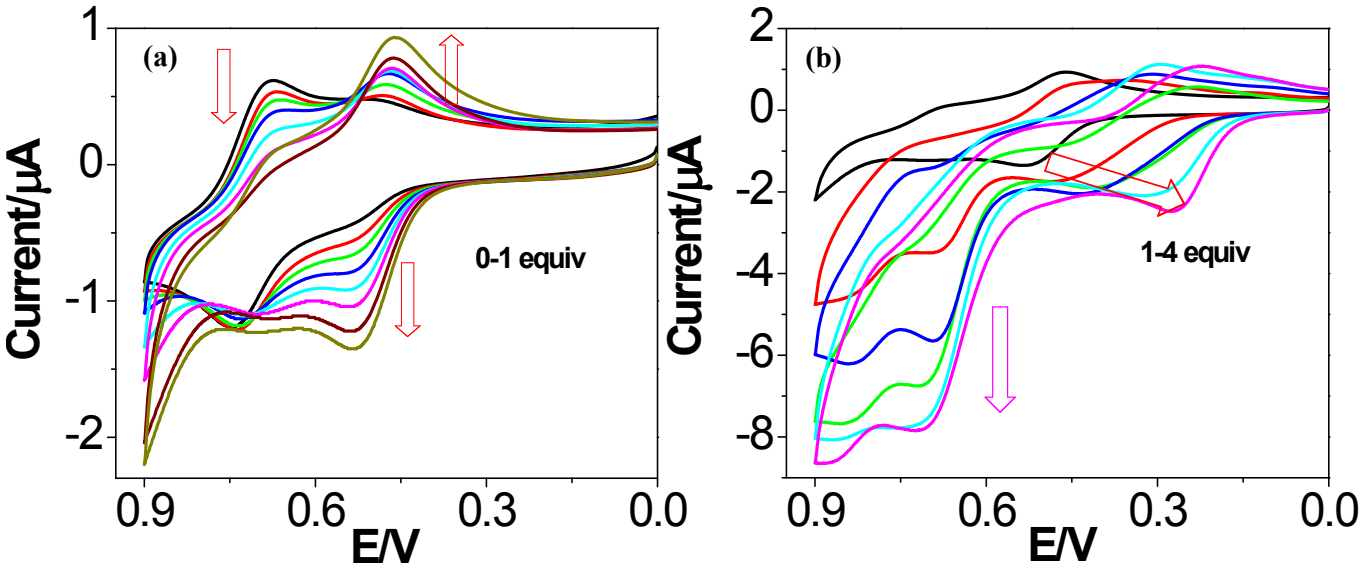

Fig. S24 Changes in the oxidation process of complex **2** in terms of CV (a and b) with incremental addition of CN^- ion in its acetonitrile solution.

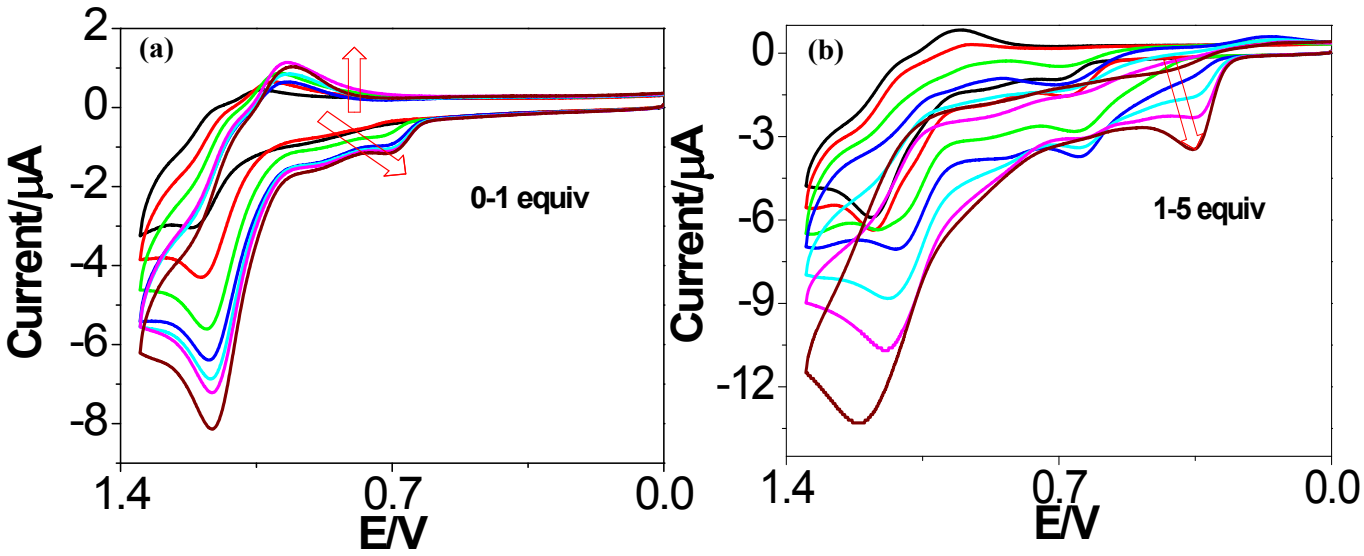

Fig. S25 Changes in the oxidation process of complex **1** in terms of CV (a and b) with incremental addition of CN^- ion in its acetonitrile solution.

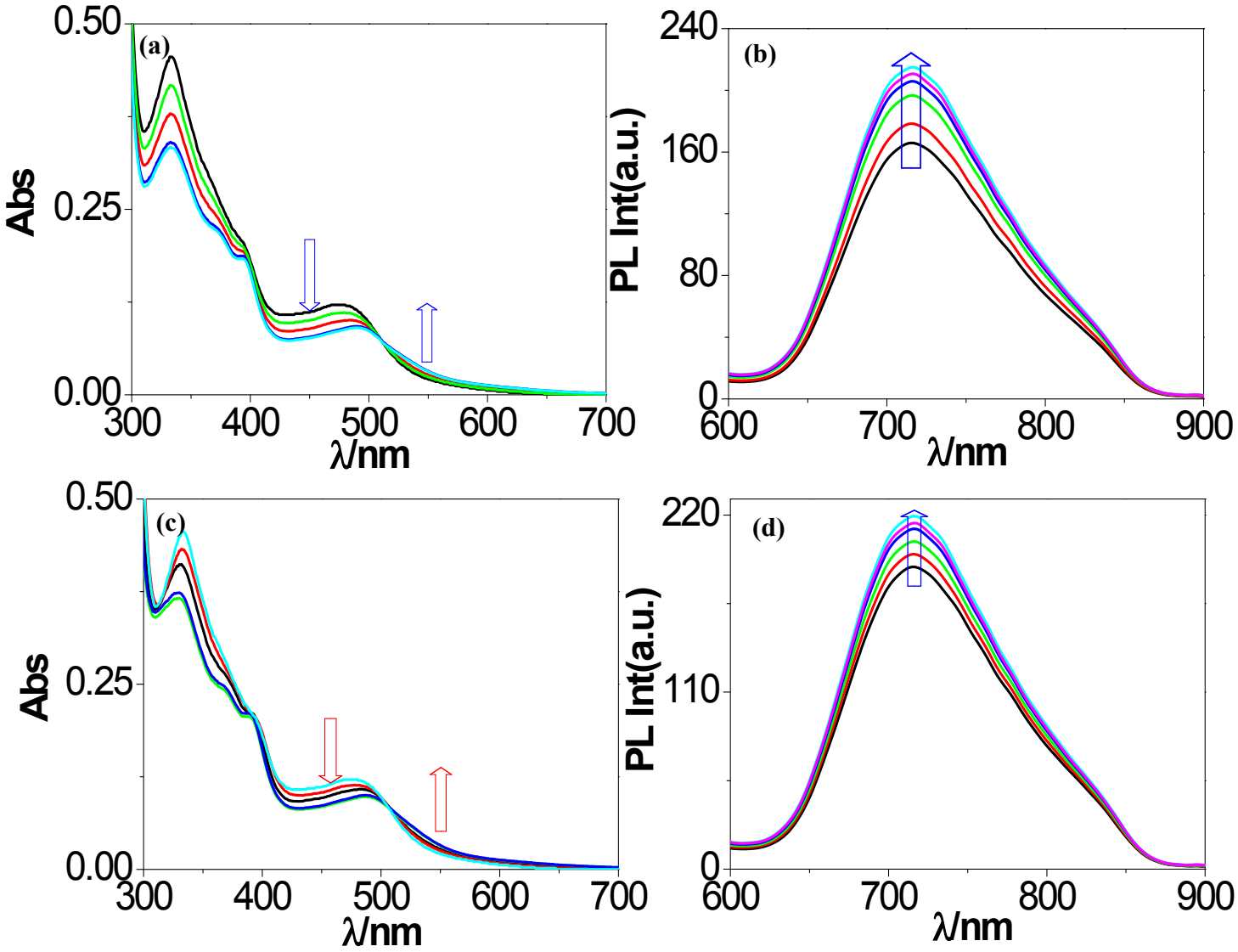

Fig. S26 Changes in UV-vis absorption (a and c) and luminescence (b and d) spectra of complex **1** in aqueous buffer solution (pH=7) upon the addition of CO_3^{2-} and S^{2-} ion respectively.

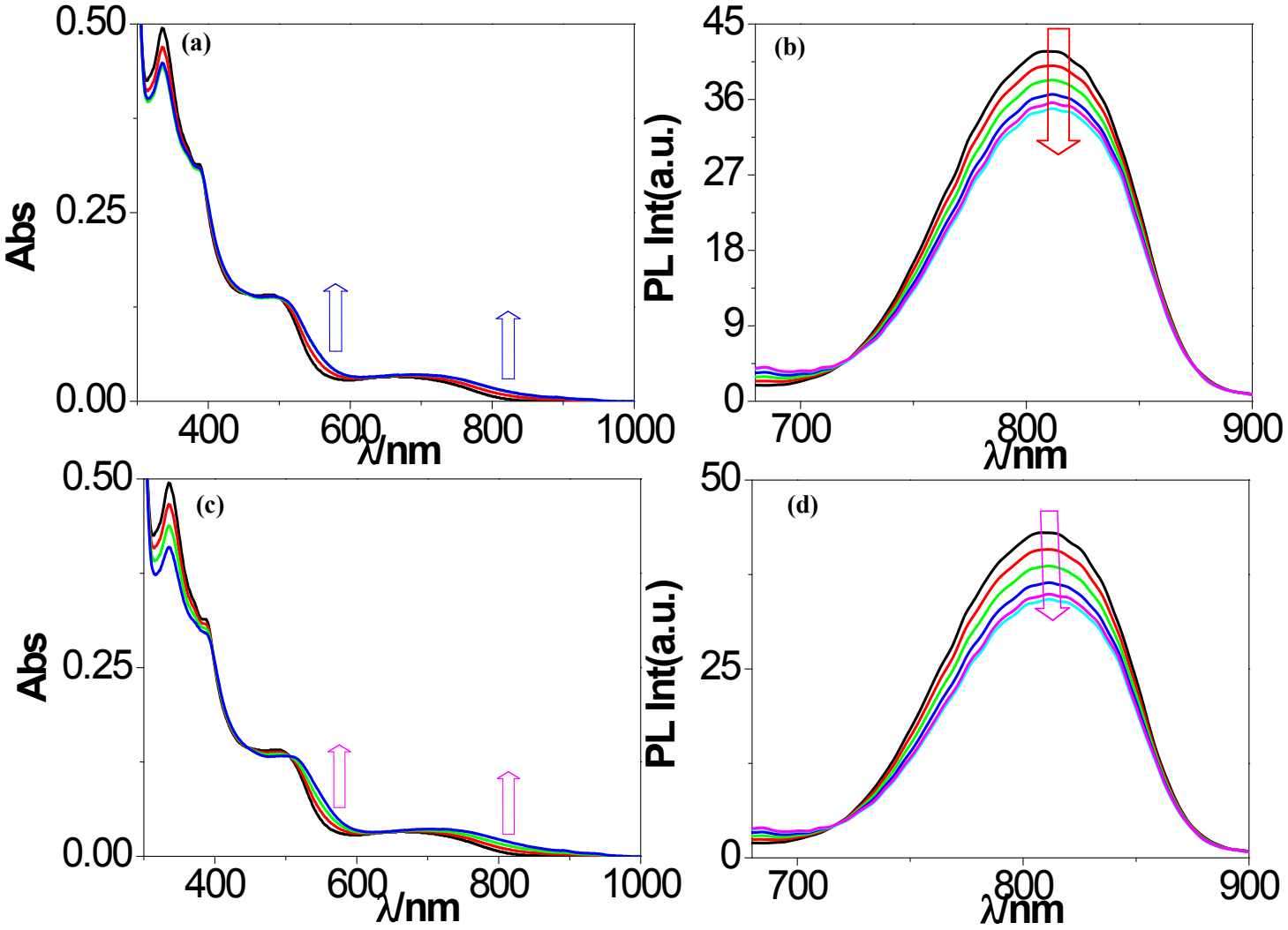

Fig. S27 Changes in UV-vis absorption (a and c) and luminescence (b and d) spectra of complex **2** in aqueous buffer solution (pH=7) upon the addition of CO_3^{2-} and S^{2-} ion respectively.

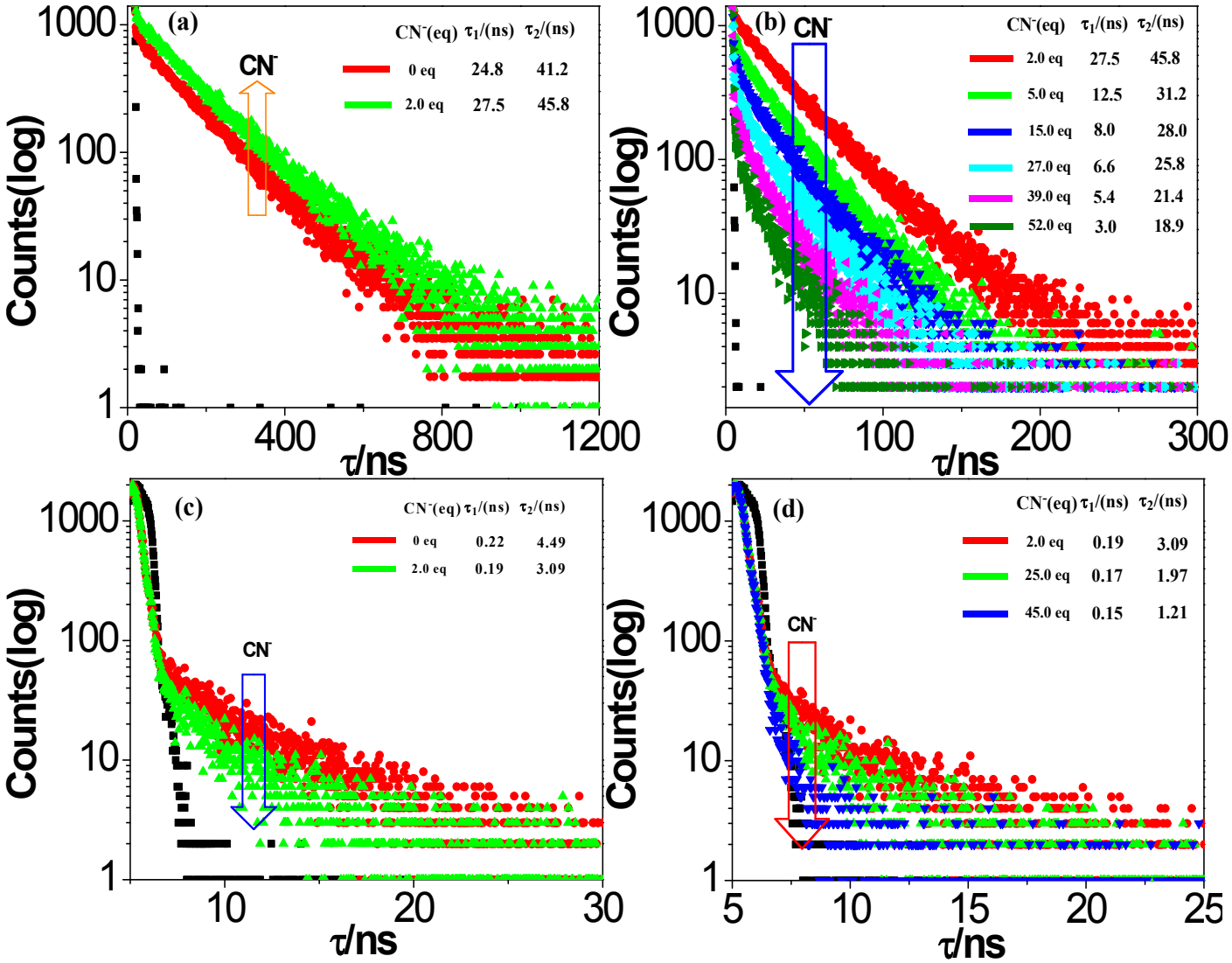

Fig. S28 Changes in the time-resolved luminescence decays for **1** (a and b) with incremental addition of CN^- (0-50 equiv) and for **2** (c and d) with CN^- (0-45 equiv) in pure aqueous medium. Insets show the lifetime values.

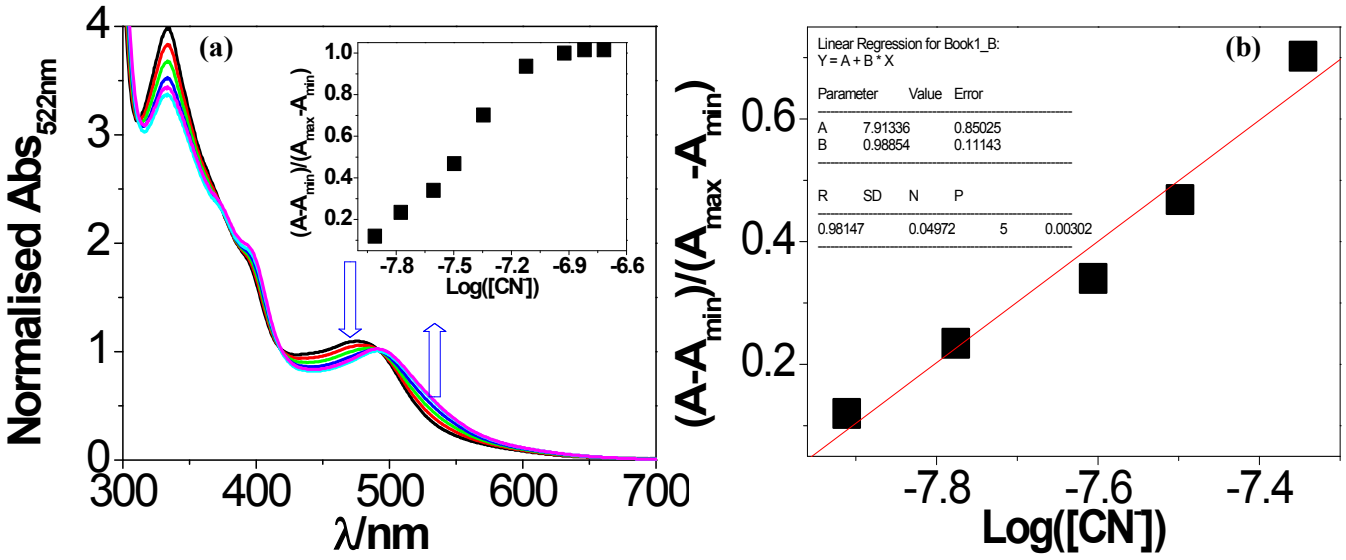

Fig. S29 (a) Absorption spectral change during the titration of **1** with CN^- in water medium, inset shows the normalized absorbance between the minimum absorbance (free complex **1**) and the maximum absorbance. (b) A plot of $(A-A_{min})/(A_{max}-A_{min})$ vs Log([CN^-]), the calculated detection limit of receptor is 1.12×10^{-8} M.

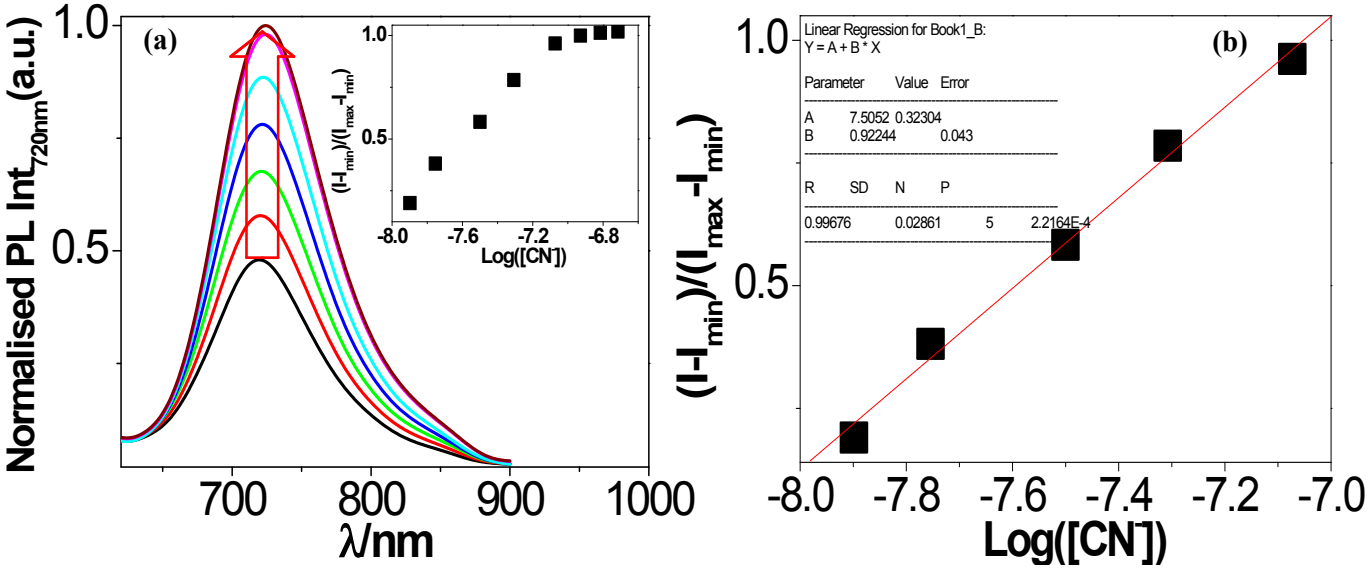

Fig. S30 (a) Fluorescence spectral change during the titration of **1** with CN^- in water medium, inset shows the normalized intensity between the minimum intensity (free complex **1**) and the maximum intensity. (b) A plot of $(I-I_{min})/(I_{max}-I_{min})$ vs Log([CN^-]), the calculated detection limit of receptor is 1.03×10^{-8} M.

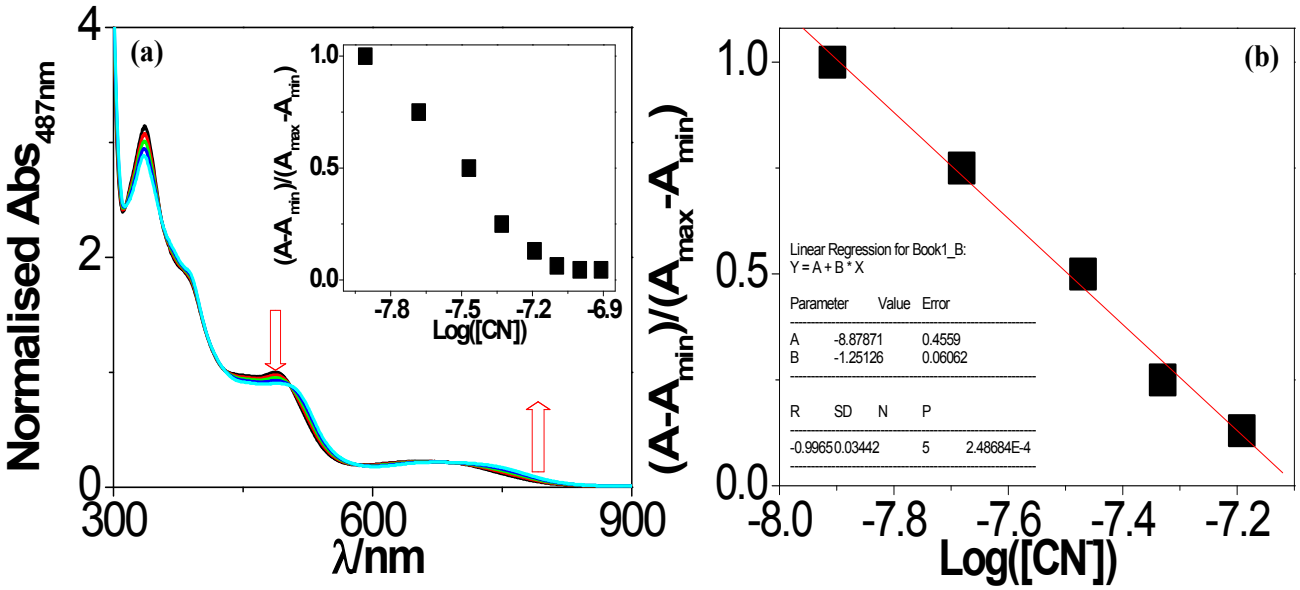

Fig. S31 (a) Absorption spectral change during the titration of **2** with CN^- in water medium, inset shows the normalized absorbance between the minimum absorbance (free complex **2**) and the maximum absorbance. (b) A plot of $(A-A_{min})/(A_{max}-A_{min})$ vs Log([CN^-]), the calculated detection limit of receptor is 1.10×10^{-8} M.

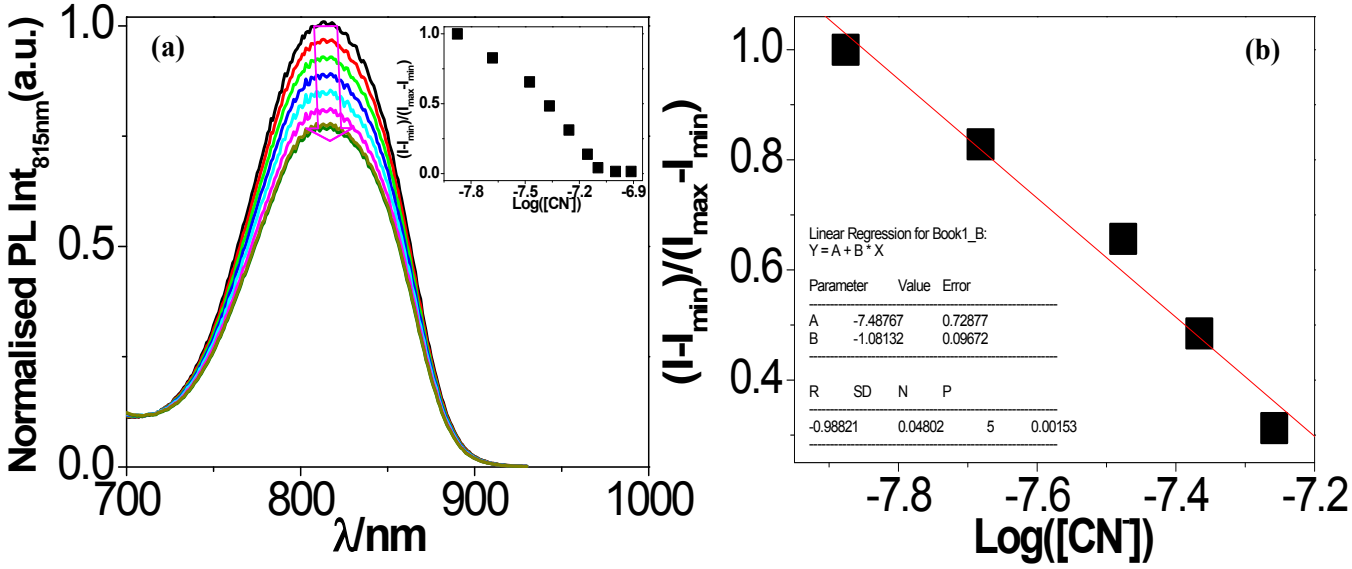

Fig. S32 (a) Fluorescence spectral change during the titration of **2** with CN^- in water medium, inset shows the normalized intensity between the minimum intensity (free complex **2**) and the maximum intensity. (b) A plot of $(I-I_{min})/(I_{max}-I_{min})$ vs Log([CN^-]), the calculated detection limit of receptor is 1.24×10^{-8} M.

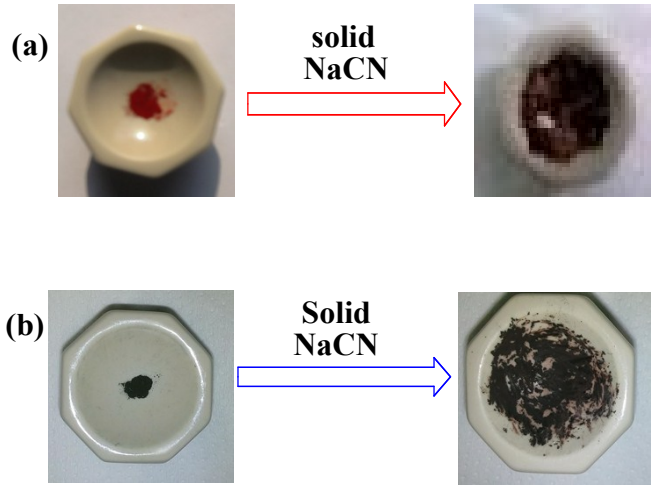

Fig. S33 Visible color changes that occur when receptor **1** and **2** (a and b respectively) are grinded mechanochemically with NaCN in solid state.

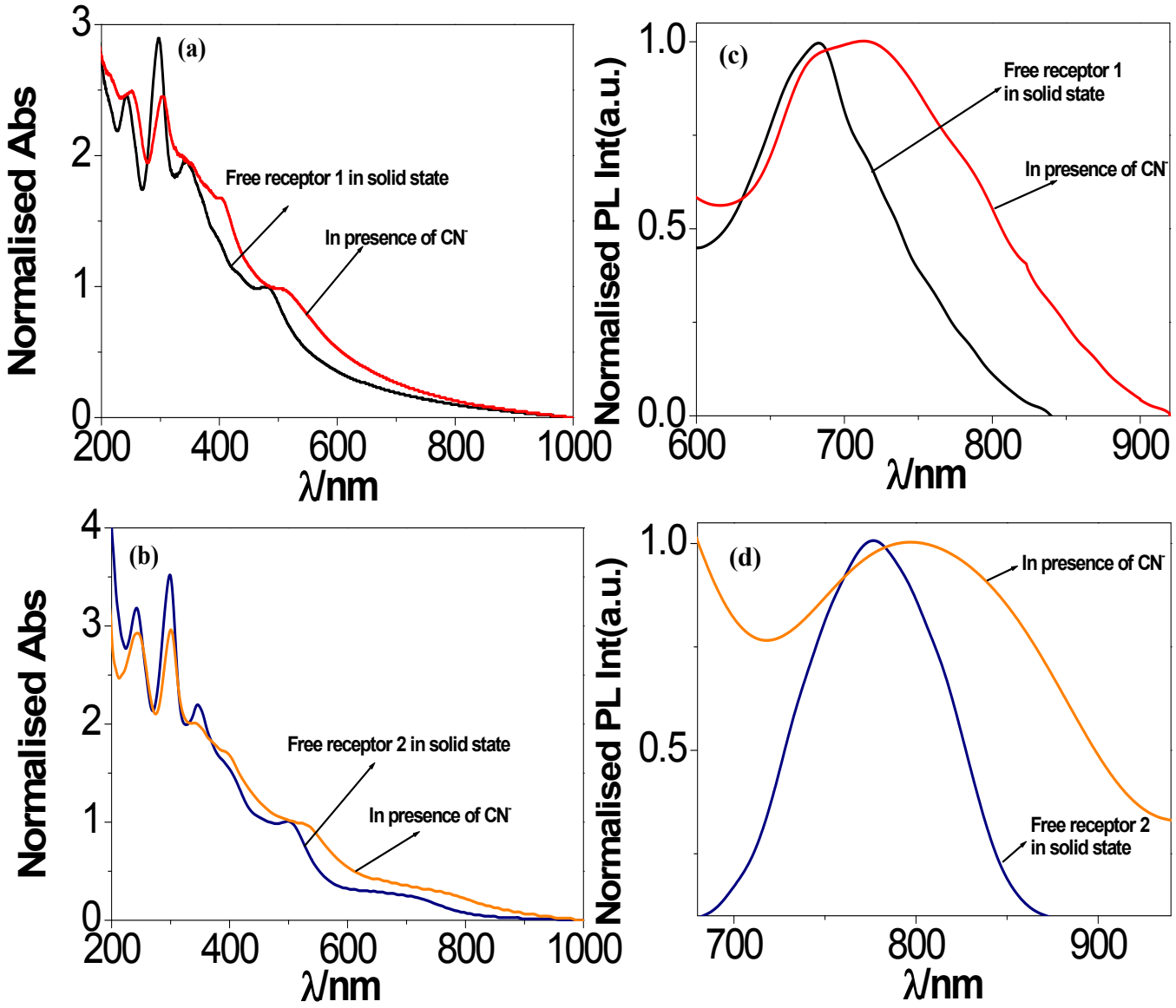

Fig. S34 Changes in UV-vis absorption (a and b) and luminescence (c and d) spectra of **1** and **2**, respectively in solid state upon grinding with CN^- ion.

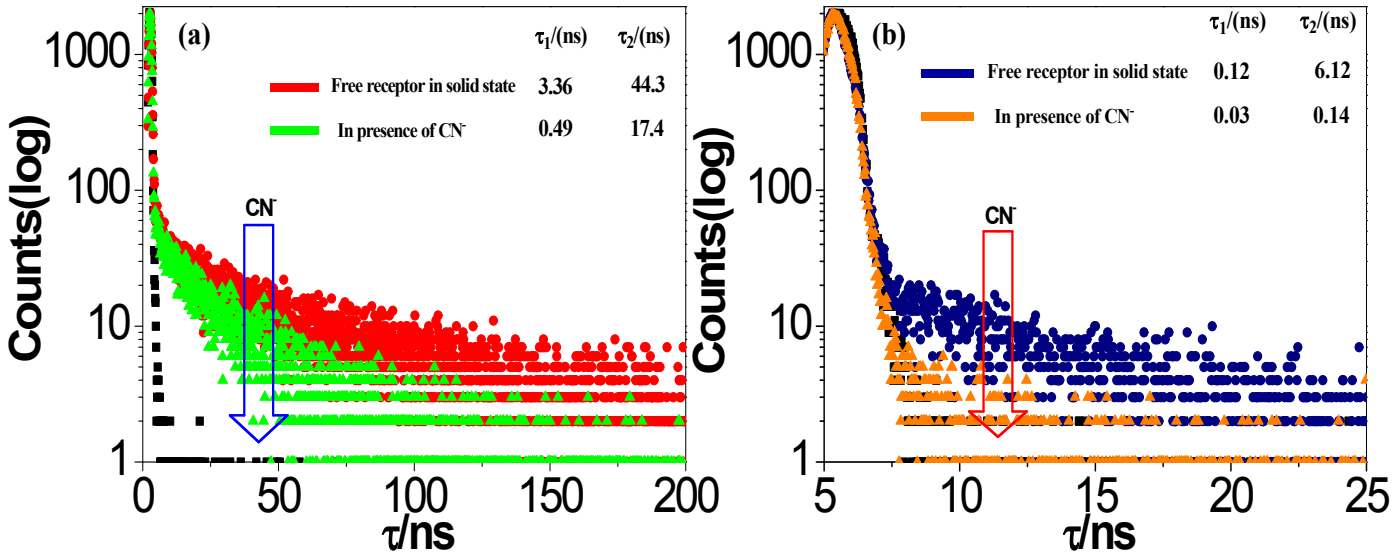

Fig. S35 Changes in the time-resolved luminescence decays for **1** (a) and **2** (b) in solid state when grinded with CN^-. Insets show the lifetime values.

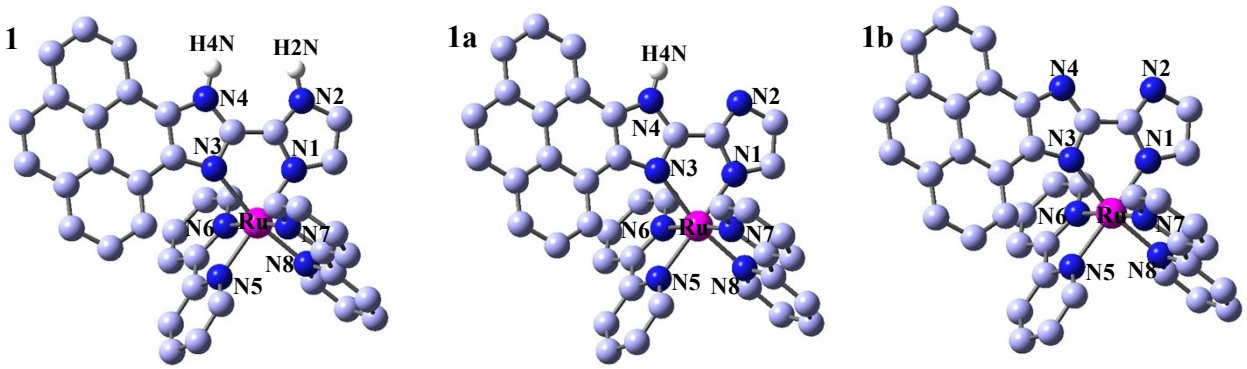

Fig. S36 Optimised geometries and labelling scheme for $[(bpy)_2Ru(Py\text{-}BiimzH_2)]^{2+}$ **(1),** $[(bpy)_2Ru(Py\text{-}BiimzH)]^{+}$ **(1a)** and $[(bpy)_2Ru(Py\text{-}Biimz)]^{0}$ **(1b)** in solution phase (using 6-31G(d) and SDD basis sets).

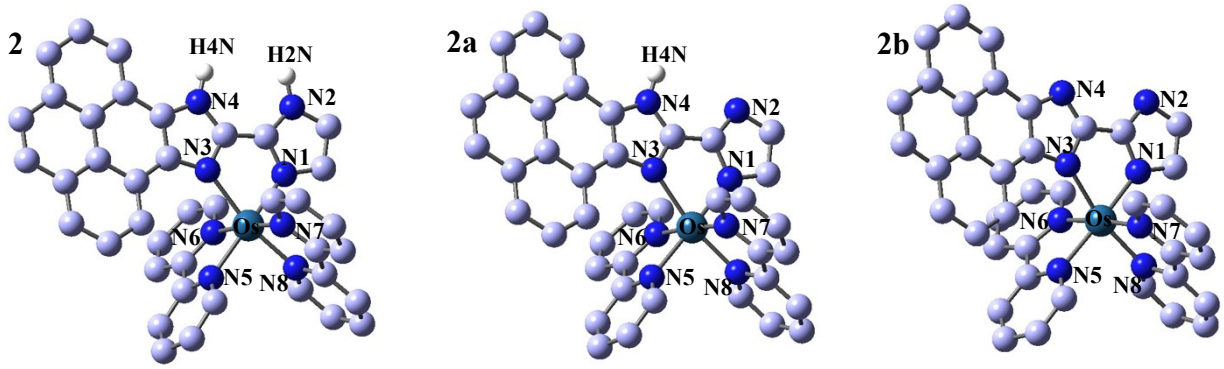

Fig. S37 Optimised geometries and labelling scheme for $[(bpy)_2Os(Py\text{-}BiimzH_2)]^{2+}$ (**2**), $[(bpy)_2Os(Py\text{-}BiimzH)]^{+}$ (**2a**) and $[(bpy)_2Os(Py\text{-}Biimz)]^{0}$ **(2b)** in solution phase (using 6-31G(d) and SDD basis sets).

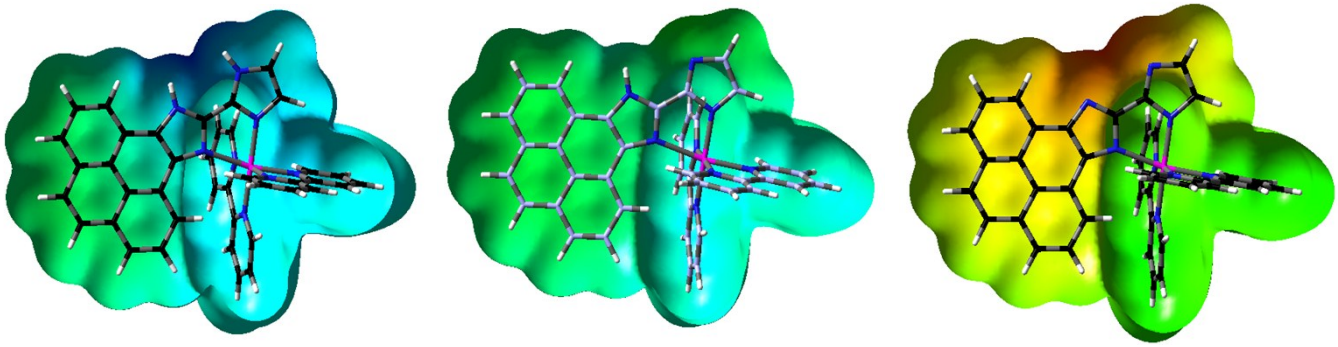

Fig. S38 Molecular electrostatic potential mapped on the isodensity surface in the ground state for $[(bpy)_2Ru(Py\text{-}BiimzH_2)]^{2+}$ (**1**), $[(bpy)_2Ru(Py\text{-}BiimzH)]^{+}$ (**1a**) and $[(bpy)_2Ru(Py\text{-}Biimz)]^{0}$ **(1b)** in the range from −4.000e-2 (red) to +4.000e-2 (blue) .

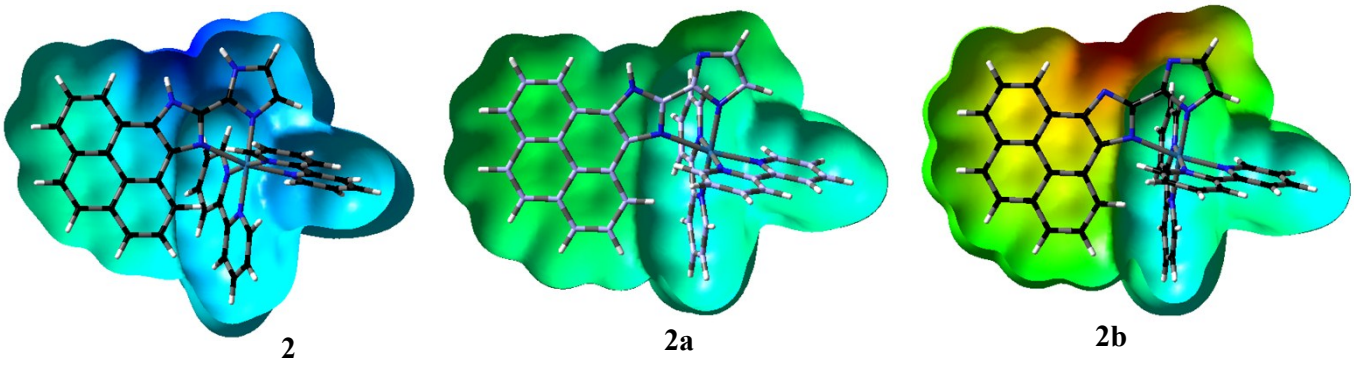

Fig. S39 Molecular electrostatic potential mapped on the isodensity surface in the ground state for $[(bpy)_2Os(Py\text{-}BiimzH_2)]^{2+}$ (**2**), $[(bpy)_2Os(Py\text{-}BiimzH)]^{+}$ (**2a**) and $[(bpy)_2Os(Py\text{-}Biimz)]^{0}$ **(2b)** in the range from −4.000e-2 (red) to +4.000e-2 (blue) .

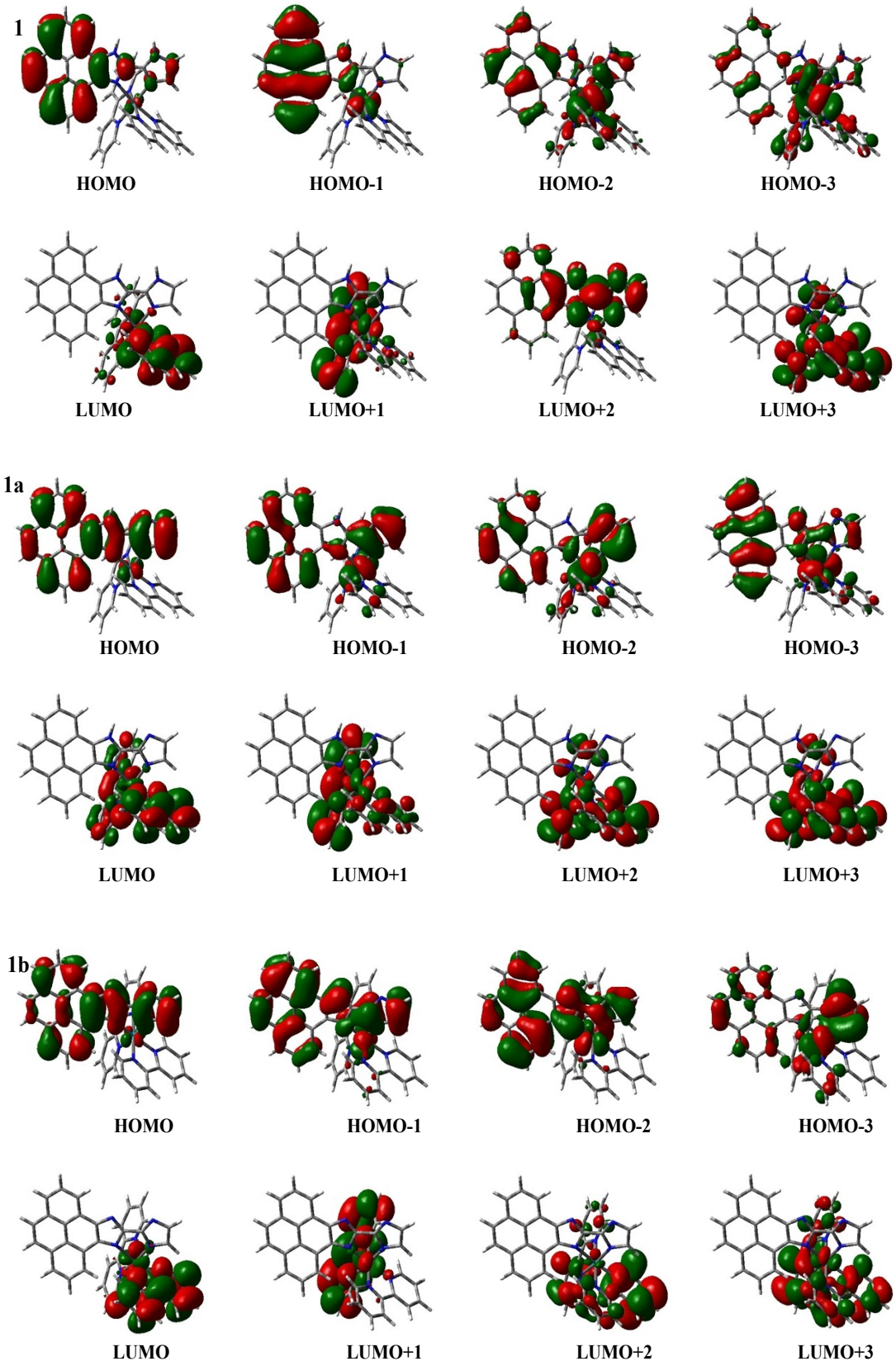

Fig. S40 Schematic drawings of the selective frontier molecular orbitals for $[(bpy)_2Ru(Py\text{-}BiimzH_2)]^{2+}$ (**1**), $[(bpy)_2Ru(Py\text{-}BiimzH)]^{+}$ (**1a**) and $[(bpy)_2Ru(Py\text{-}Biimz)]^{0}$ **(1b)** in solution phase (using 6-31G(d) and SDD basis sets).

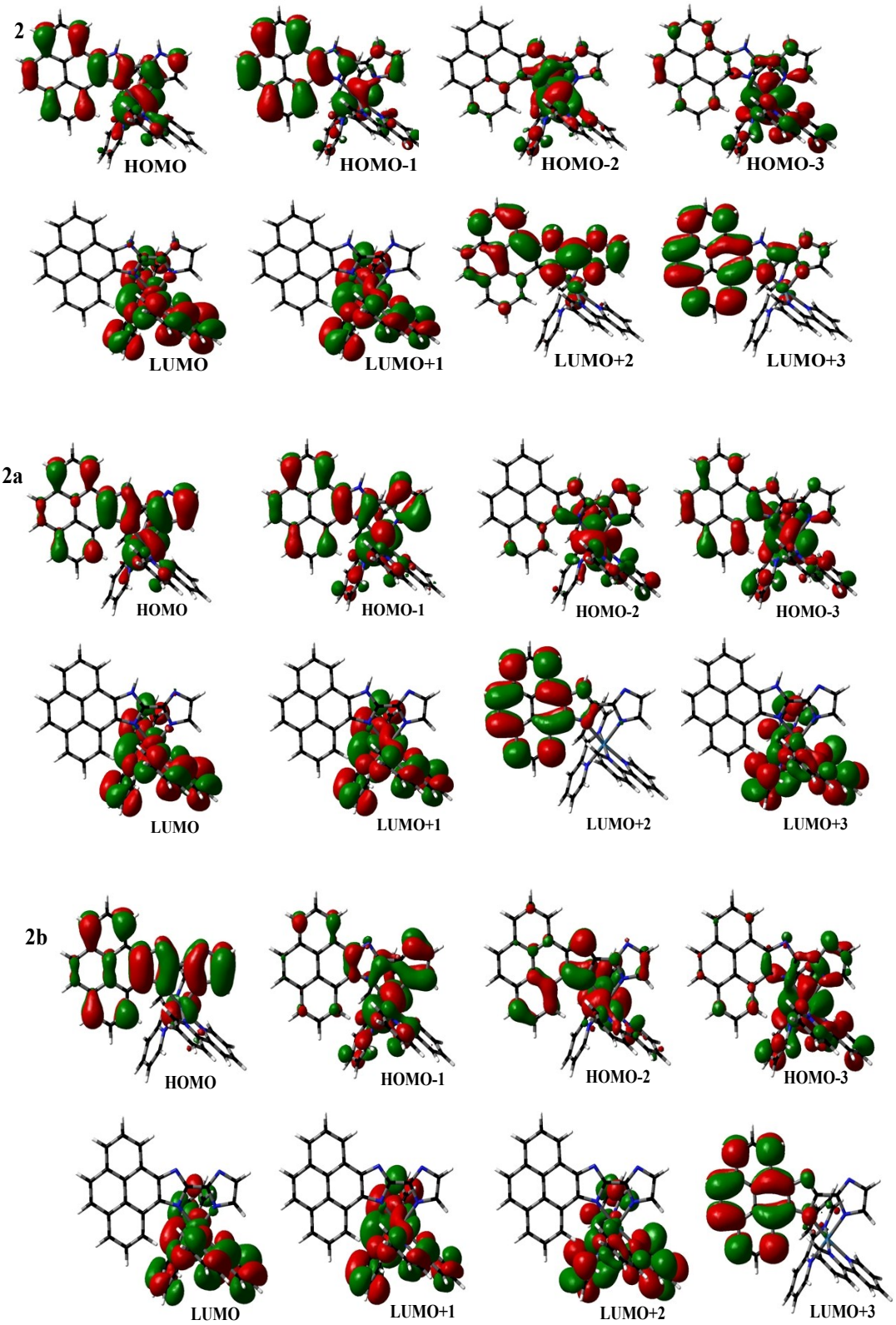

Fig. S41 Schematic drawings of the selective frontier molecular orbitals for $[(bpy)_2Os(Py\text{-}BiimzH_2)]^{2+}$ (**1**), $[(bpy)_2Os(Py\text{-}BiimzH)]^{+}$ (**1a**) and $[(bpy)_2Os(Py\text{-}Biimz)]^{0}$ **(1b)** in solution phase(using -31G(d) and SDD basis sets).

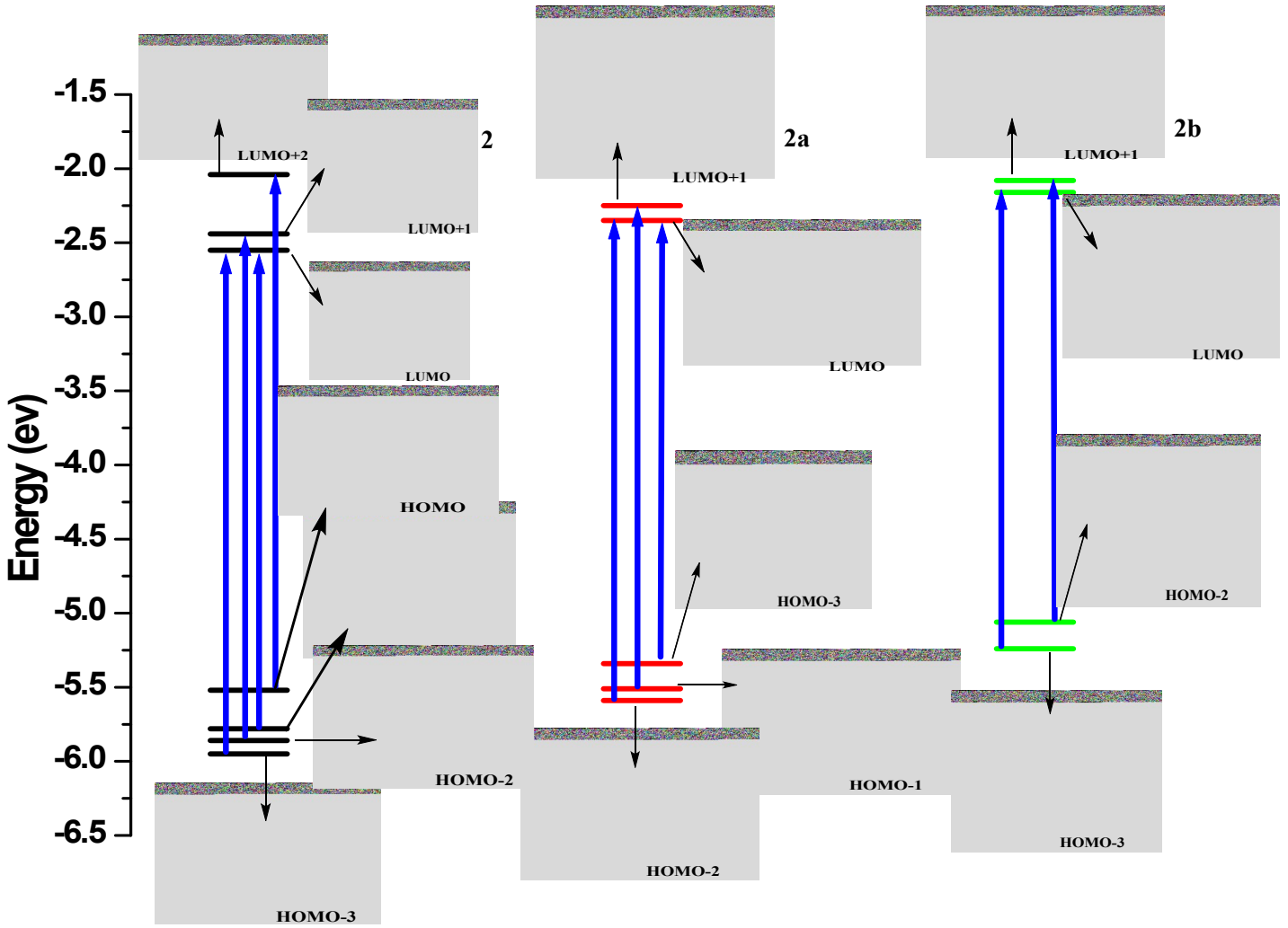

Fig. S42 Energy level diagrams depicting the dominant transitions that comprise the lowest-energy absorption band for $[(bpy)_2Os(Py\text{-}BiimzH_2)]^{2+}$ (**2**), $[(bpy)_2Os(Py\text{-}BiimzH)]^{+}$ (**2a**) and $[(bpy)_2Os(Py\text{-}Biimz)]$ **(2b)** in acetonitrile (using 6-31G(d) and SDD basis sets).

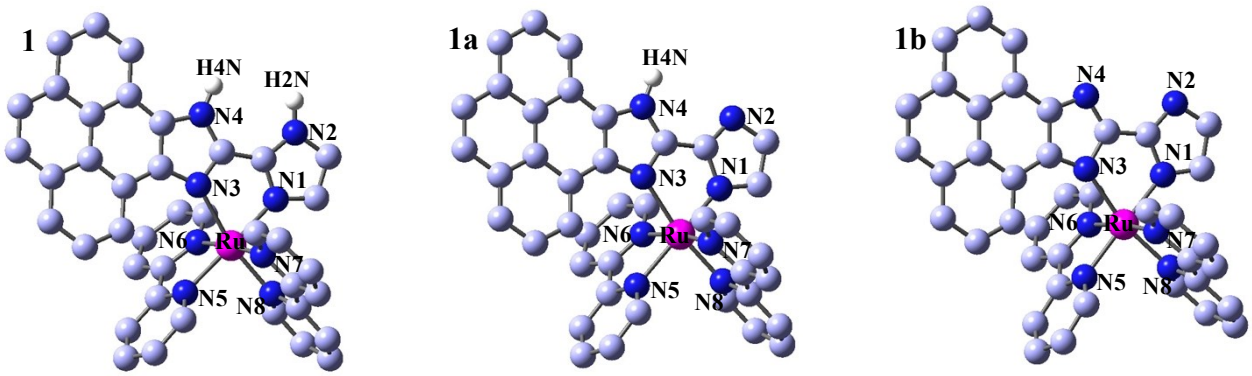

Fig. S43 Optimised geometries and labelling scheme for $[(bpy)_2Ru(Py\text{-}BiimzH_2)]^{2+}$ (**1**), $[(bpy)_2Ru(Py\text{-}BiimzH)]^{+}$ (**1a**) and $[(bpy)_2Ru(Py\text{-}Biimz)]^{0}$ **(1b)** in triplet excited state (using 6-31G(d) and SDD basis sets).

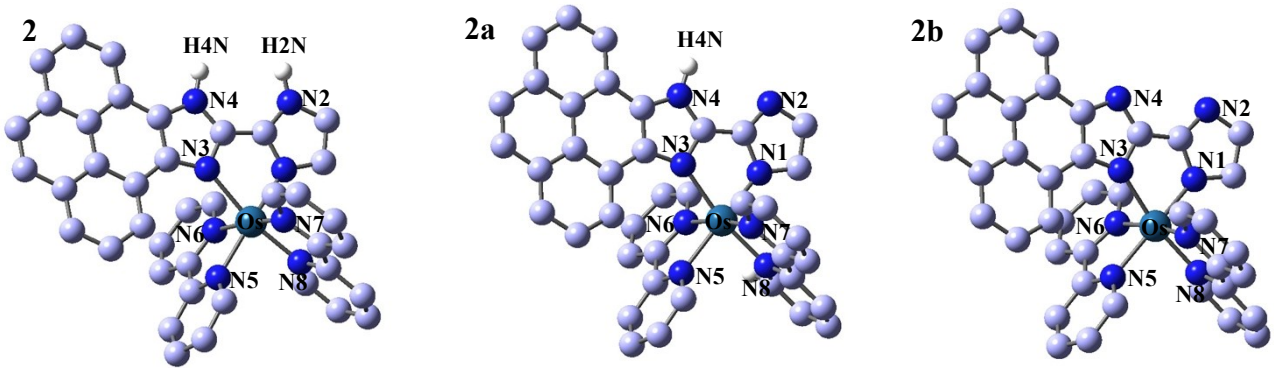

Fig. S44 Optimised geometries and labelling scheme for $[(bpy)_2Os(Py\text{-}BiimzH_2)]^{2+}$ (**2**), $[(bpy)_2Os(Py\text{-}BiimzH)]^{+}$ (**2a**) and $[(bpy)_2Os(Py\text{-}Biimz)]^{0}$ **(2b)** in triplet excited state (using 6-31G(d) and SDD basis sets).

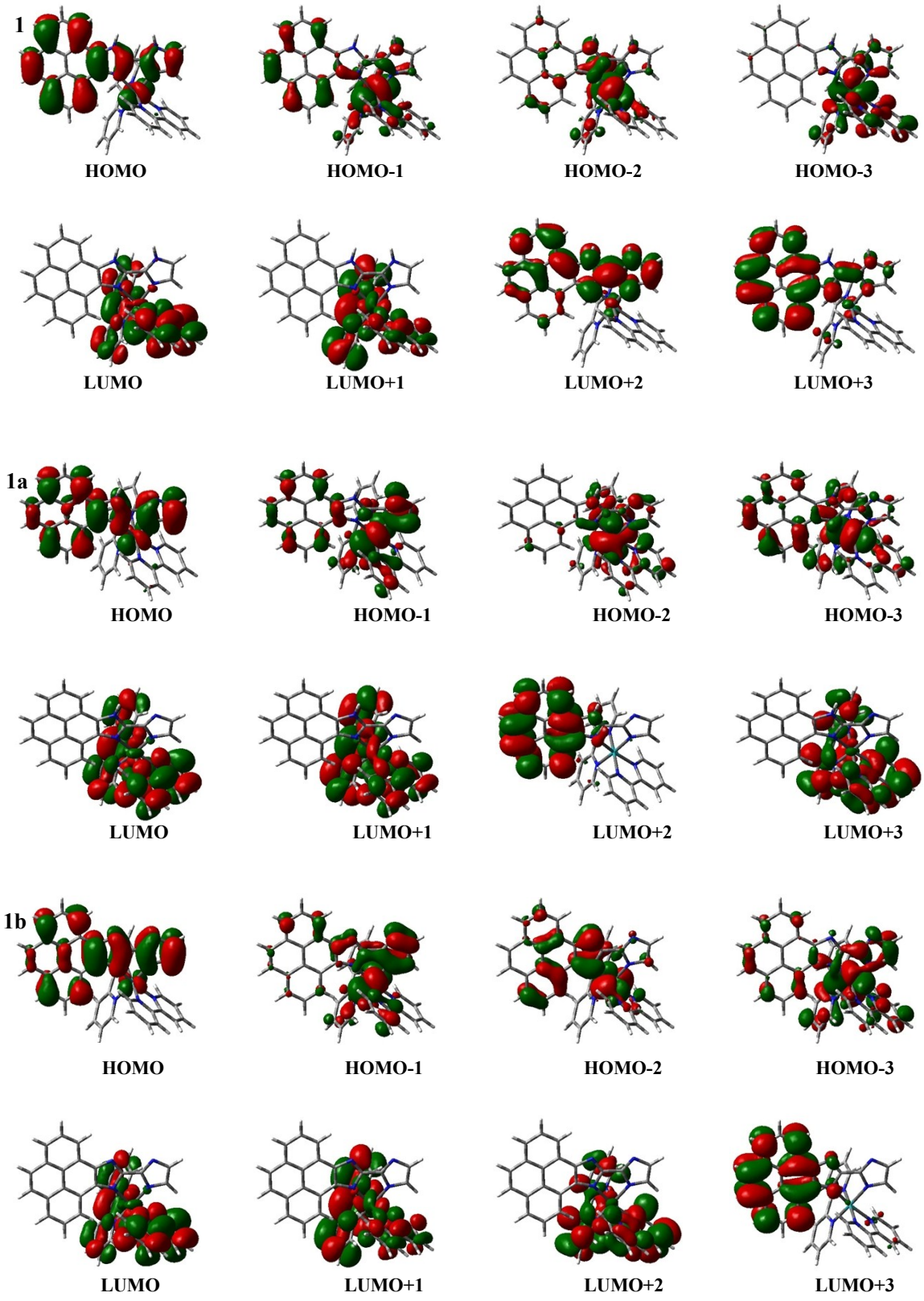

Fig. S45 Schematic drawings of the selective frontier molecular orbitals for $[(bpy)_2Ru(Py\text{-}BiimzH_2)]^{2+}$ **(1),** $[(bpy)_2Ru(Py\text{-}BiimzH)]^{+}$ **(1a)** and $[(bpy)_2Ru(Py\text{-}Biimz)]^{0}$ **(1b)** in triplet excited state (using 6-31G(d) and SDD basis sets).

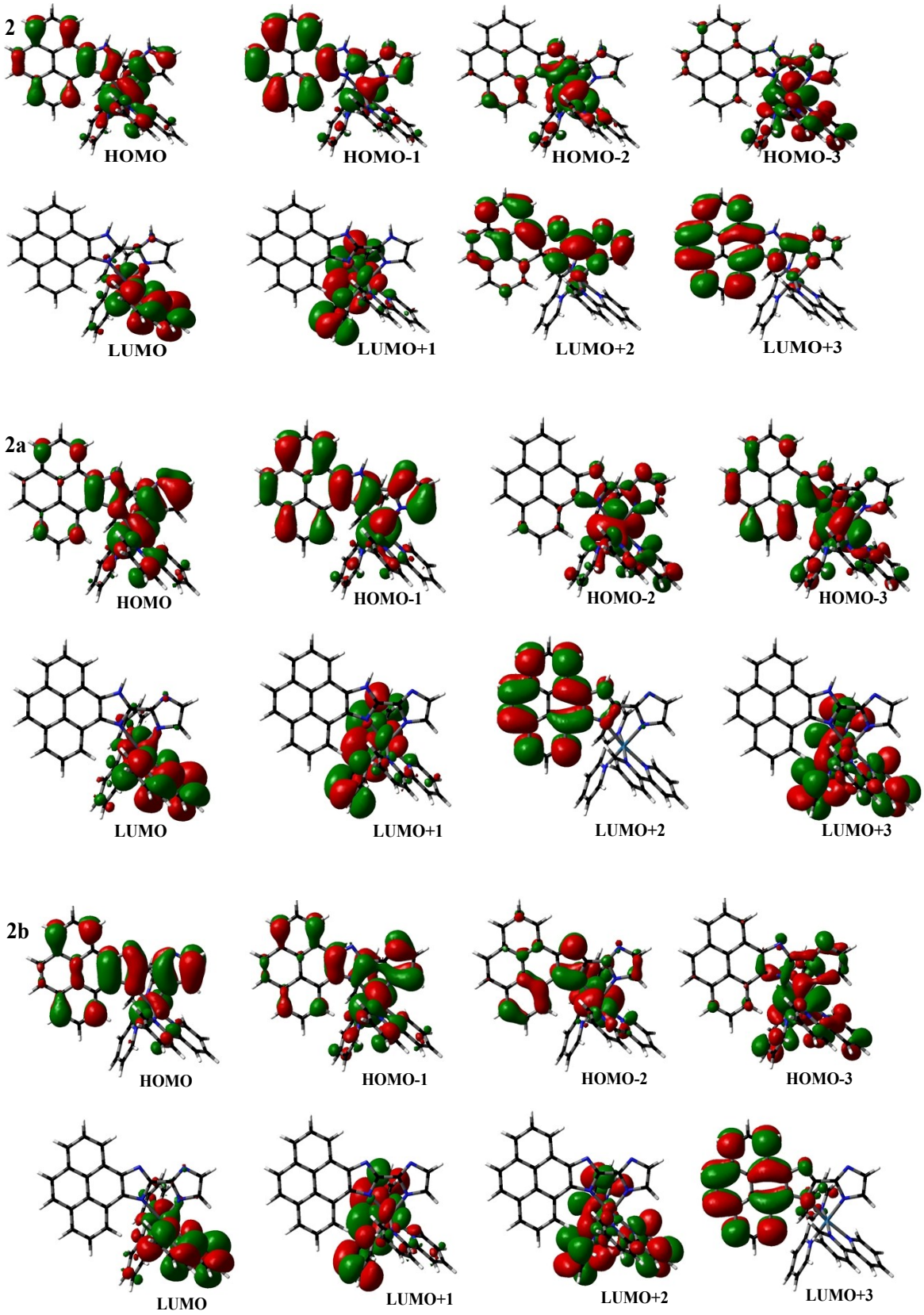

Fig. S46 Schematic drawings of the selective frontier molecular orbitals for $[(bpy)_2Os(Py\text{-}BiimzH_2)]^{2+}$ (**2**), $[(bpy)_2Os(Py\text{-}BiimzH)]^{+}$ (**2a**) and $[(bpy)_2Os(Py\text{-}Biimz)]^{0}$ **(2b)** in triplet excited state (using 6-31G(d) and SDD basis sets).

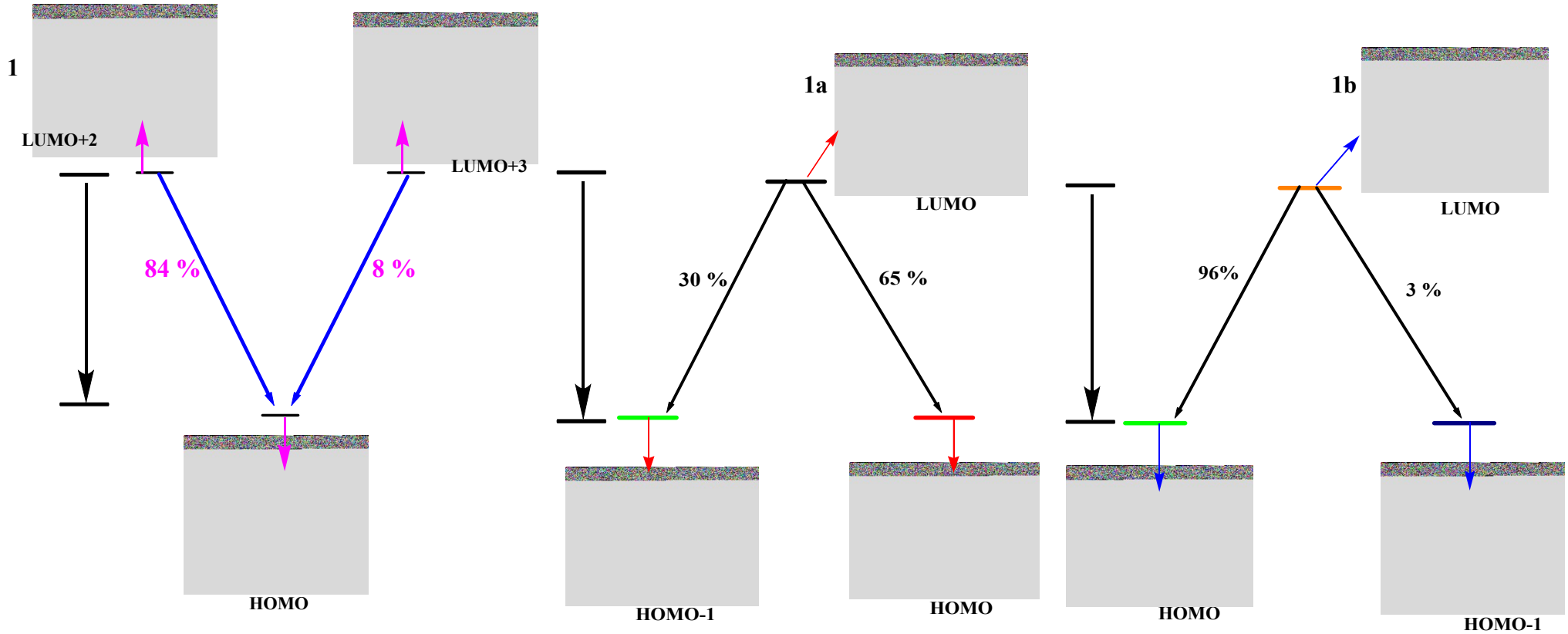

Fig. S47 Calculated single electron transitions for the emissions of T_1 states for $[(bpy)_2Ru(Py\text{-}BiimzH_2)]^{2+}$ (**1**), $[(bpy)_2Ru(Py\text{-}BiimzH)]^{+}$ (**1a**) and $[(bpy)_2Ru(Py\text{-}Biimz)]^{0}$ **(1b)** (using 6-31G(d) and SDD basis sets).

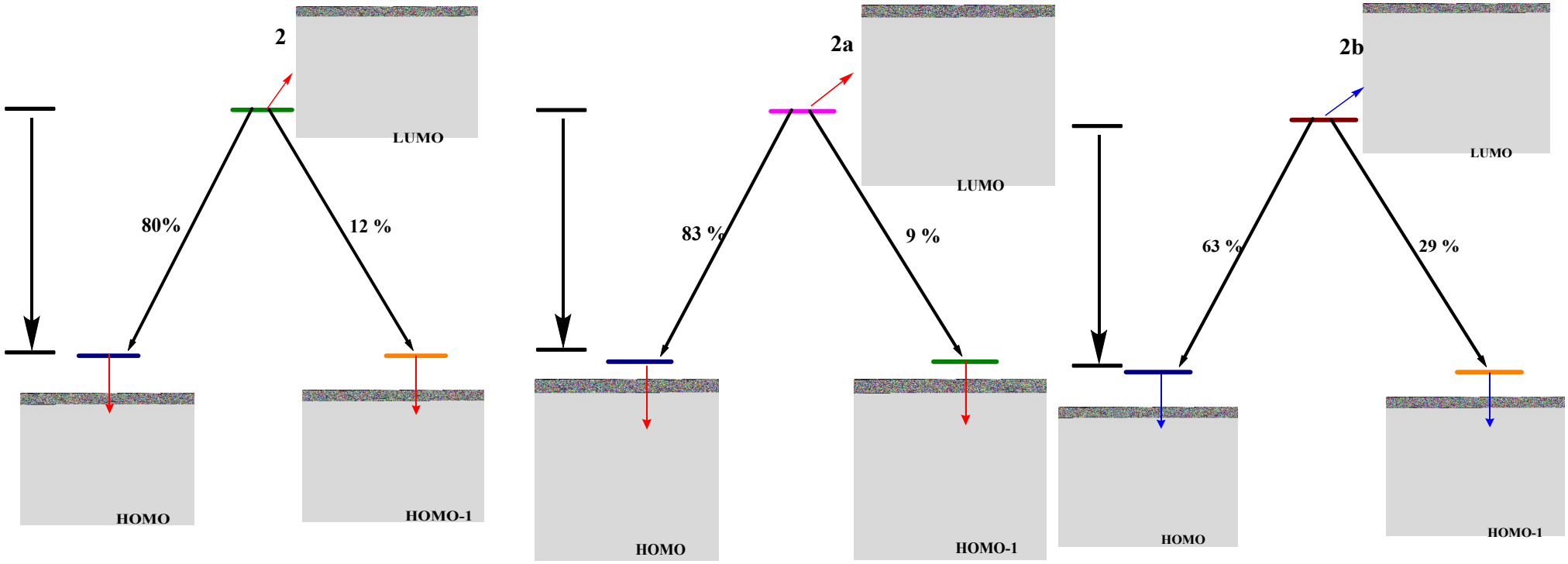

Fig. S48 Calculated single electron transitions for the emissions of T_1 states for $[(bpy)_2Os(Py\text{-}BiimzH_2)]^{2+}$ (**2**), $[(bpy)_2Os(Py\text{-}BiimzH)]^{+}$ (**2a**) and $[(bpy)_2Os(Py\text{-}Biimz)]^{0}$ **(2b)** (using 6-31G(d) and SDD basis sets).

References

(S1) (a) K. Nakamaru, *Bull. Chem. Soc. Jpn*. 1982, **55**, 1639 and references cited therein; (b) J. N. Demas and G. A.Crosby, *J. Am. Chem. Soc.* 1971, **93**, 2841; (c) J. van Houten and R. J. Watts, *J. Am. Chem. Soc.* 1976, **98**, 4853.

(S2) Schneider, H.-J.; Yatsimirsky, A. *Principles and Methods in Supramolecular Chemistry*; John Wiley & Sons: England, 2000, 142.

(S3) SAINT (version 6.02), SADABS (version 2.03); Bruker AXS Inc.: Madison, WI, 2002.

(S4) SHELXTL, (version 6.10); Bruker AXS Inc.: Madison, WI, 2002.

(S5) Sheldrick, G. M. SHELXL-97, *Program for the Refinement of crystal Structures*; University of Göttingen: Göttingen, Germany, 1997.

(S6) PLATON; Spek, A. L. *J. Appl. Cryst.* 2003, **36,** 7-13.

(S7) M. J. Frisch, G. W. Trucks, H. B. Schlegel, G. E. Scuseria, M. A. Robb, J. R. Cheeseman, G. Scalmani, V. Barone, B. Mennucci, G. A. Petersson, H. Nakatsuji, M. Caricato, X. Li, H. P. Hratchian, A. F. Izmaylov, J. Bloino, G. Zheng, J. L. Sonnenberg, M. Hada, M. Ehara, K. Toyota, R. Fukuda, J. Hasegawa, M. Ishida, T. Nakajima, Y. Honda, O. Kitao, H. Nakai, T. Vreven, J. A. Montgomery, J. E.Jr.; Peralta, F. Ogliaro, M. Bearpark, J. J. Heyd, E. Brothers, K. N. Kudin, V. N.Staroverov, R. Kobayashi, J. Normand, K. Raghavachari, A. Rendell, J. C. Burant, S. S. Iyengar, J. Tomasi, M. Cossi, N. Rega, J. M. Millam, M. Klene, J. E. Knox, J. B. Cross, V. Bakken, C. Adamo, J. Jaramillo, R. Gomperts, R. E. Stratmann, O. Yazyev, A. J. Austin, R. Cammi, C. Pomelli, J. W. Ochterski, R. L. Martin, K. Morokuma, V. G. Zakrzewski, G. A. Voth, P. Salvador, J. J. Dannenberg, S. Dapprich, A. D. Daniels, Ö. Farkas, J. B. Foresman, J. V. Ortiz, J. Cioslowski and D. J. Fox, Gaussian 09, revision A.02; Gaussian Inc.: Wallingford, CT, 2009.

(S8) A. D. Becke, *J. Chem. Phys.*, 1993**, 98**, 5648-5652.

(S9) C. T. Lee, W. T. Yang and R. G. Parr, *Phys. Rev. B*, 1988, **37**, 785-789.

(S10) (a) D. Andrae, U. Haeussermann, M. Dolg, H. Stoll and H. Preuss, *Theor. Chim. Acta.* 1990, **77**, 123. (b) P. Fuentealba, H. Preuss, H. Stoll and L. V. Szentpaly, *Chem. Phys. Lett*. 1989, **89**, 418.

(S11) P. J. Hay and W. R. Wadt, *J. Chem. Phys.* 1985, **82**, 299-310.

(S12) M. E. Casida, C. Jamorski, K. C. Casida and D. R. Salahub, *J. Chem. Phys.* 1998, **108**, 4439-4449.

(S13) R. E. Stratmann, G. E. Scuseria and M. J. Frisch, *J. Chem. Phys.* 1998, **109**, 8218-8224.

(S14) V. A. Walters, C. M. Hadad, Y. Thiel, S. D. Colson, K. B. Wiberg, P. M. Johnson and J. B. Foresman, *J. Am. Chem. Soc.* 1991, **113**, 4782-4791.

(S15) (a) J. Tomasi, B. Mennucci and R. Cammi, *Chem. Rev*. 2005, **105**, 2999−3094. (b) M. Cossi, G. Scalmani, N. Rega and V. Barone, *J. Chem. Phys*. 2002, **117**, 43−54.

(S16) M. Caricato, B. Mennucci, J. Tomasi, F. Ingrosso, R. Cammi, S. Corni and G. Scalmani, *J. Chem. Phys*. 2006, **124**, 124520-124533.

(S17) B. Mennucci, C. Cappelli, C. A. Guido, R. Cammi and J. Tomasi, *J. Phys. Chem. A* 2009, **113**, 3009-3020.

(S18) R. II. Dennington, T. Keith and J. Millam, *Gauss View 3*; Semichem, Inc.: Shawnee Mission, KS, 2007.

(S19) N. M. O Boyle, A. L. Tenderholt and K. M. Langner, *J. Comput. Chem*. 2008, **29**, 839-845.